

Hydroclimatic variability of opposing late Pleistocene climates in the Levant revealed by deep Dead Sea sediments

Yoav Ben Dor^{1,2}, Francesco Marra^{1,2}Marra^{2,3}, Moshe Armon¹Armon², Yehouda Enzel¹Enzel², Achim Brauer^{3,4}Brauer^{4,5}, Markus Julius Schwab³Schwab⁴, Efrat Morin¹Morin²

¹ Geological Survey of Israel, 32 Yesha'ayahu Leibowitz, Jerusalem 9692100, Israel

² The Fredy and Nadine Herrmann Institute of Earth Sciences, The Hebrew University of Jerusalem, Jerusalem, 9190501, Israel

³ Institute of Atmospheric Sciences and Climate, National Research Council of Italy, Bologna, 40129, Italy

⁴ Section Climate Dynamics and Landscape Evolution, GFZ German Research Centre for Geosciences, Telegrafenberg, 14473, Potsdam, Germany

⁵ Department of Earth Sciences, Potsdam University, Karl-Liebknecht-Straße 24/25, 14476, Potsdam, Germany

Correspondence to: Yoav Ben Dor (Yoav.Bendor1@mail.huji.ac.il)

Abstract. Annual and decadal-scale hydroclimatic variability describes key characteristics that are embedded into climate insitu in situ, and is of specifically prime importance specifically in subtropical regions. The study of hydroclimatic variability is therefore crucial to understand its manifestation asand implications on climate derivatives such as hydrological phenomena and water availability. However, the study of this variability from modern records is limited due to their relatively short span, whereas model simulations relying on modern dynamics could misrepresent some of its aspects. Here we study annual to decadal hydroclimatic variability in the Levant using two sedimentary sections covering ~700 years each, from the depocenter of the Dead Sea, which has been continuously recording environmental conditions since the late-Pleistocene. We focus on the two series of annually deposited laminated intervals (i.e., varves) representingthat represent two episodes of opposing mean climates, deposited during MIS2 lake-level rise and fall during at ~27 and 18 Kaka, respectively. These two series comprise alternations of authigenic aragonite that precipitated during summer and flood-borne detrital laminae deposited by winter floods. Within this record, aragonite laminae form a proxy of annual inflow and the extent of epilimnion dilution, whereas detrital laminae compriseare comprised of sub-laminae that recorddeposited by individual flooding events. The two series depict distinct characteristics with increased mean and variance of annual inflow and flood frequency during “wetter”, with respect to the relatively “drier”, conditions, reflected by opposite lake-level changes. In addition, decades of intense flood frequency (clusters) are identified (e.g., clusters), depicting the insitu in situ impact of shifting centennial-scale climate regimes, which are particularly pronounced during wetter conditions. The combined application of multiple time series analyses suggests that the studied episodes are characterized by weak and non-significant periodicyclical components of sub-decadal frequencies. CombiningThe interpretation of these observations withtheusing modern synoptic-scale hydroclimatology suggests that Pleistocene climate changes resulted in shifts of the dominance of the key synoptic systems that govern rainfall, annual inflow and flood frequency in the eastern Mediterranean Sea over centennial time-scales.

1 Introduction

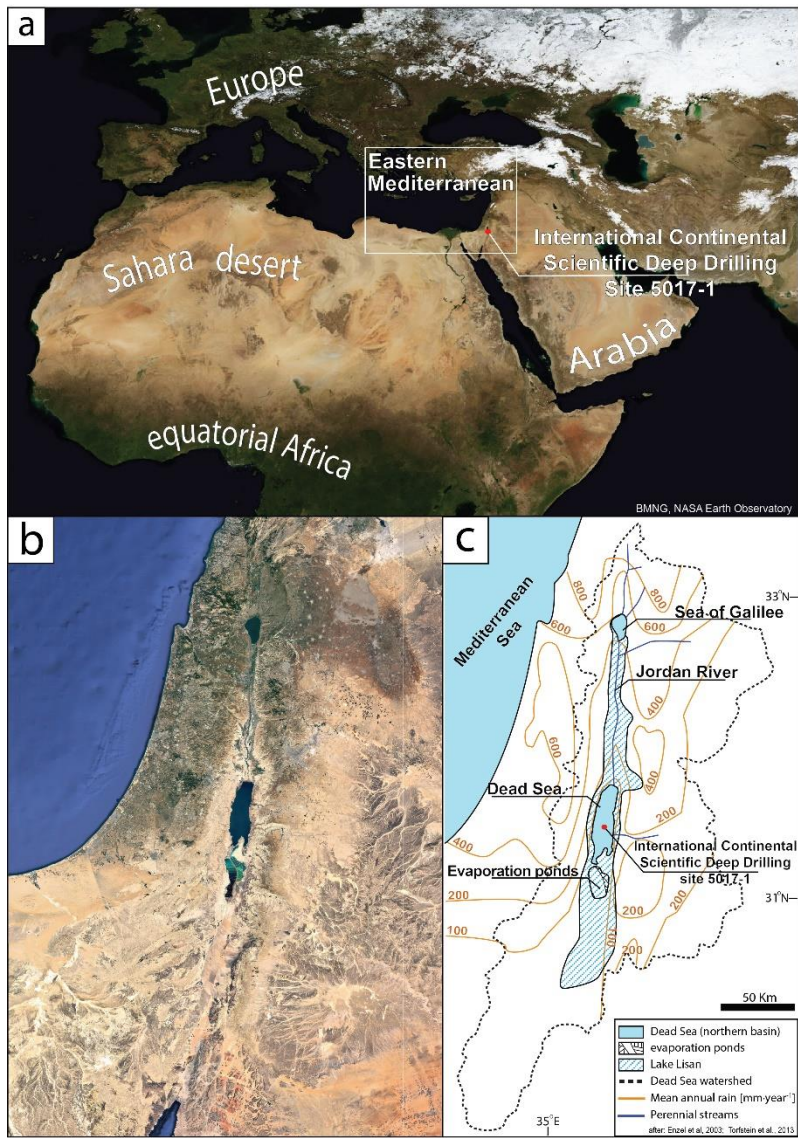
Human activity relies on continuous availability of freshwater, which in turn depends on the interaction of climatic, environmental and hydrologic processes. Water availability is particularly crucial in drylands and subtropical regions that cover significant portions of the Earth’s surface and host nearly 20% of the world’s population (e.g., Safriel et al., 2005). In these areasregions, hydroclimatic variability at seasonal, annual and decadal scales bear significant impact on water availability that could result in growing water stress as populations growhuman population grows (e.g., Luck et al., 2015; Luo et al., 2015). It is therefore crucial to understand how hydroclimatic variability in drylands and Mediterranean regions could be affected by climate changes, such as those humanity faces in the upcoming decades (Peleg et al., 2015; Seager et al., 2019; Zappa et al.,

2015; IPCC, 2021). However, because the study of hydroclimatic variability requires high resolution measurements, that currently only cover several decades, the interpretation and the quantification of relationships between trends, oscillations and ~~transition~~ transitions between climatic states, as well as their impact on the local water cycle ~~insitu~~, are ~~still~~ limited and are therefore ~~still~~ debated (e.g., Morin, 2011; Serinaldi et al., 2018); (e.g., Morin, 2011; Serinaldi et al., 2018). Furthermore, the impacts of climate change on short-term phenomena such as individual storms and floods, which bear substantial influence on the ~~insitu~~ ~~in situ~~ water cycle in the Mediterranean ~~regions~~ Sea, are harder to determine from the available short historical records because the extent of available data does not adequately capture the full diversity of possible hydroclimatic states (e.g., Armon et al., 2018; Greenbaum et al., 2010; Tarolli et al., 2012; Metzger et al., 2020). Because palaeohydrologic archives often record centennial and millennial intervals at various resolutions (e.g., Allen et al., 2020; Baker, 2008; Brauer et al., 2008; Redmond et al., 2002; Witt et al., 2017), they have the potential to improve our understating of how climate change is manifested locally into short-term hydroclimatic variability (e.g., Ahlborn et al., 2018; Swierczynski et al., 2012). Nevertheless, this requires continuous high-resolution archives, which are rare, especially in sub-tropical ~~arid~~ terrestrial environments (e.g., Zolitschka et al., 2015).

The subtropical Levant (e.g., eastern Mediterranean) exhibits a sharp climatic gradient ranging from subhumid Mediterranean in the north (Köppen-Geiger classification), where precipitation is focused in winter ~~and transition seasons~~ months (December~~October~~-May), to hyperarid climate zones in the south (N-S; Kottek et al., 2006), ~~and~~ whereas summers (June-September) are dry and hot. Because the main source of moisture to the region is the Mediterranean Sea, the orographic effect of the central mountainous belt of Israel ~~results in~~ superimposes an ~~abrupt~~ additional sharp W-E climatic gradient, where the eastern parts are substantially drier than its ~~eastern~~ western parts (Fig. 1; Kushnir et al., 2017). Under these seasonal conditions, the region is sensitive to spatiotemporal changes in global circulation, where slight modifications could bear substantial impact on ~~the~~ its hydrological cycle and ~~on~~ water availability (Fig. 1; e.g., Held and Soden, 2006; Luck et al., 2015; Shohami et al., 2011; Tamarin-Brodsky and Kaspi, 2017; Drori et al., 2021). The interaction of ~~—~~ substantial seasonality and the abovementioned climatic gradients (N-S and E-W) over the eastern Mediterranean further ~~obscure~~ obscures the impacts of climatic ~~changes~~ change on intra- and inter-annual hydroclimatic variability in the wetter Mediterranean regions ~~surrounding the Mediterranean Sea~~, as they ultimately stem from the frequency and properties of discrete extra-tropical Mediterranean cyclones (i.e., Mediterranean\Cyprus Lows\Cyclones; e.g., Campins et al., 2011; Enzel et al., 2003; Flocas et al., 2010; Saaroni et al., 2010; Ziv et al., 2004; Armon et al., 2020).

In this study, two high-resolution sequences of annually-deposited laminations (i.e., varves) of the Dead Sea deep drilling project (DSDDP) ~~obtained from the Dead Sea depocenter within the framework of the international continental scientific drilling program (ICDP; e.g., Neugebauer et al., 2014) are analyzed~~ from the depocenter of the Dead Sea within the framework of the international continental scientific drilling program (ICDP; e.g., Neugebauer et al., 2014; Torfstein et al., 2013b) are analysed to determine hydroclimatic variability in the southern Levant under contrasting late Pleistocene global and regional climate changes, recorded by independently-determined lake level trends (i.e., mean “wetter” vs. “drier” conditions; Fig. 2; e.g., Bartov et al., 2003; Torfstein et al., 2013a; Torfstein and Enzel, 2017). Two laminated segments were continuously sampled for thin-~~sections~~ section preparation, and ~~analyzed~~ analysed using microfacies analyses in high-resolution and multiple time-series analyses in order to address the following questions: (a) Can any significant differences between the two studied episodes recording opposing climatic trends be identified? (b) Do the series depict significant intra-series transitions indicative of hydroclimatic regime shifts? (c) Do the studied sequences (or parts of them) record any ~~periodic~~ oscillatory or cyclical components of ~~spectral bands~~ preferred time scales (e.g., interannual, decadal, multi-decadal components)? (d) ~~Do~~ Does any of the ~~identified periodic~~ cyclical components (partially) resemble the ~~periodicity~~ time scales of known global teleconnection patterns (e.g., the North Atlantic Oscillation, NAO; Seager et al., 2019; Black, 2012)?² i.e., can aspects of the modern

hydroclimatic variability assist in interpreting dominant aspects of hydroclimatic variability during past climate changes such as [periodic](#)~~ecyclical~~ components [of preferred time scales](#)?



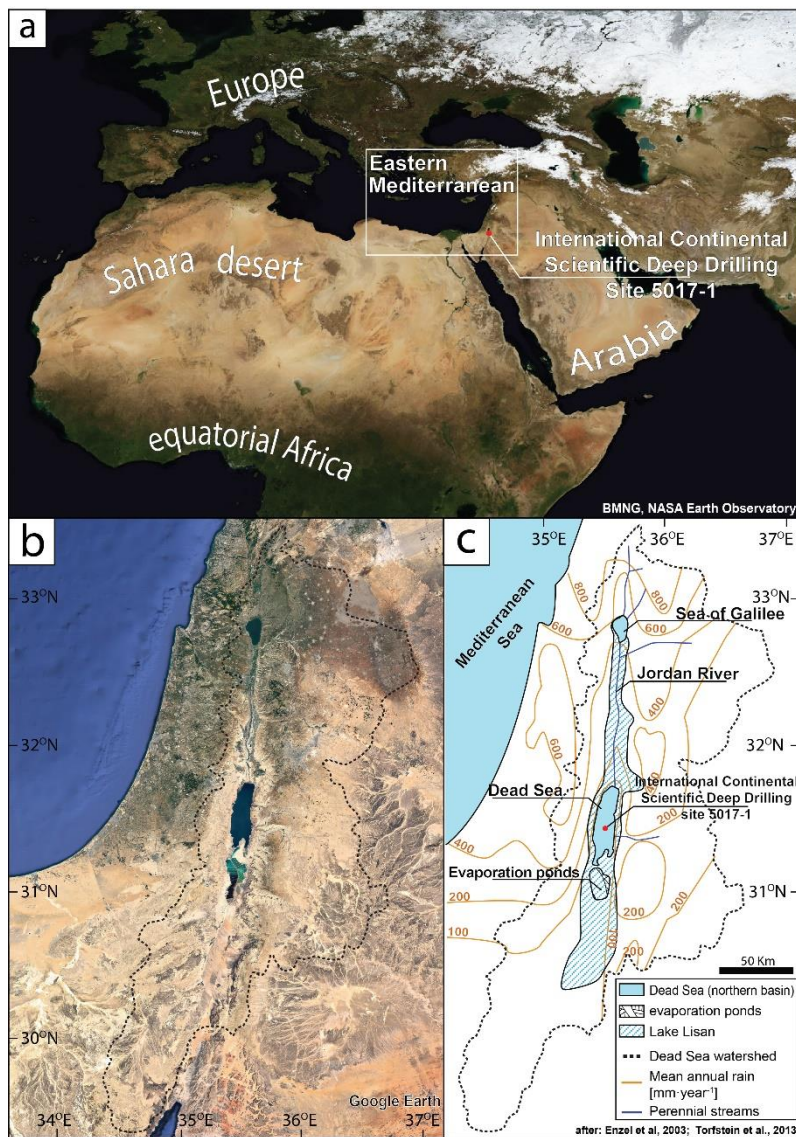


Figure 1 - a) Satellite image of the Mediterranean Sea and its surroundings surrounding depicting the pivotal location of the ICDP-DSDDP site 5017-1 on the seam of global climate belts (extracted from The Blue Marble Next Generation, NASA's Earth Observatory; Stöckli et al., 2005). b) Satellite image of the eastern Mediterranean depicting the sharp climatic gradient between the Mediterranean climate in the north (mean annual precipitation $>1000 \text{ mm}\cdot\text{yr}^{-1}$) and the hyper-arid south (mean annual precipitation $<50 \text{ mm}\cdot\text{yr}^{-1}$); image extracted from Google Earth). c) The Dead Sea watershed and the extent of Lake Lisan during the last glacial maximum (lake level $\sim 170 \text{ m bmsl}$; $\sim 260 \text{ m}$ above modern level) with modern mean annual precipitation (after Enzel et al., 2003; Torfstein et al., 2013a).

100 2 Geological, hydrological, and climatological settings

The Dead Sea is the recent and modern member of a series of waterbodies filling the deepest terrestrial depression on Earth along the central part of the Dead Sea transform since the late Miocene (e.g., Garfunkel, 1981; Garfunkel and Ben-Avraham, 1996; Waldmann et al., 2017). Because the Dead Sea is a terminal lake, changes in Dead Sea level are directly linked to precipitation fluctuations over its watershed (e.g., Morin et al., 2019), and its reconstructed lake levels are therefore utilized as a “mega palaeo-rain gauge” (Enzel et al., 2003), recording the integrated impacts of environmental and climatic conditions on watershed hydrology (Bartov et al., 2003; Bookman et al., 2006; Machlus et al., 2000; Torfstein and Enzel, 2017). These impacts are propagated into the lake's sedimentary record and are reflected by lithological transitions from sequences of alternating aragonite and detrital laminae that are deposited during (and facies; Machlus et al., 2000) laminae that are deposited during episodes of relatively high lake stands and positive water budget (Fig. 2; e.g., Ben Dor et al., 2019; Neugebauer et al.,

110 2014; Torfstein et al., 2013b), to halite (e.g., Palchan et al., 2017; Sirota et al., 2017) or gypsum during drawdowns and droughts (Torfstein et al., 2008).

~~Although~~ Although the full wet season lasts from October to May, ~65% of precipitation over the Dead Sea watershed is limited to the mild and wet winters (December-February). At the northern, ~~and~~-wetter part of the region, >90% of precipitation is delivered by low pressure systems originating from the Mediterranean Sea (i.e., Mediterranean Lows), whereas during ~~summers~~ summers (June-~~August~~September), large-scale atmospheric subsidence results in stable dry and hot conditions (Goldreich, 2012; Kushnir et al., 2017; Tyrlis et al., 2013; Kelley et al., 2012). On average, the northern and western parts of the Dead Sea watershed are characterized by increased precipitation and lower temperatures, resulting in a pronounced climatic N-S gradient. The average temperatures during winter range between ~10 and ~20°C, whereas during summer, temperatures range from ~20 to ~35°C, in the northern and southern parts of the Dead Sea watershed, respectively (Israel Meteorological Service, 2021). Mean annual precipitation in the southernmost hyperarid region is under 50 mm·yr⁻¹, usually delivered ~~during~~ within less than 10 rainy days, whereas in the mountainous region at the ~~north~~ northernmost headwaters, it exceeds 1000 mm·yr⁻¹ and ~~spreads~~ spreads over more than 75 rainy days (Goldreich, 2012; Sharon and Kutiel, 1986). Precipitation over the southern ~~part of the~~ Levant is characterized by substantial spatiotemporal variability, depicting scattered, spotty, and intense convective rain, ~~and the few observed precipitation events in the southern arid parts are separated by prolonged dry intervals ranging from weeks to years~~ (Sharon, 1972). ~~The few observed precipitation events in the southern arid parts are separated by prolonged dry intervals ranging from weeks to months.~~ The pronounced orographic effect of the Judean ~~mountains~~ Mountains, which separate the Lower Jordan Valley from the Mediterranean Sea, substantially decreases rainfall as storms progress eastward towards the Dead Sea basin, thus ~~resulting in~~ forming a sharp E-W precipitation gradient, which decreases from >500 mm·yr⁻¹ in Jerusalem to <100 mm·yr⁻¹ at the Dead Sea, over less than 50 km. East of the Dead Sea, the mountainous topography of the Jordanian escarpment increases annual precipitation to over 400 mm·yr⁻¹ at its highest parts (Fig. 1; Enzel et al., 2003)

Available records indicate that the ~~modern~~ climatic gradients gradient over the Dead Sea watershed was ~~similar~~ maintained during the late Pleistocene (Keinan et al., 2019; Enzel et al., 2008). These observations ~~determine also constrain~~ water and sediment transport paths into the lake, where the main water source is its Mediterranean ~~climate~~ climate zone ~~to~~ in the north (Fig. 1; e.g., Enzel et al., 2003; Ziv et al., 2006), where annual precipitation and water supply largely depend on the spatiotemporal properties and the frequency of ~~extra-tropical cyclonic systems~~ Mediterranean Lows during winter (~~i.e. Mediterranean Lows~~; Campins et al., 2011; Goldreich, 2004; Saaroni et al., 2010). Detrital sediments are delivered to the ICDP 5017 coring site at the depocenter of the Dead Sea lake primarily by ~~flash~~ floods from adjacent streams (e.g., Nehorai et al., 2013; Ben Dor et al., 2018), and debris flows (Ahlborn et al., 2018). ~~Whereas~~ While floods are ~~generally~~ associated with Mediterranean Lows (Dayan and Morin, 2006; Kahana et al., 2002; Tsvieli and Zangvil, 2005), ~~debris flows, are associated with~~ and rarely by disturbances of the subtropical jet stream (i.e., Tropical Plumes; Armon et al., 2018; Enzel et al., 2012; Tubi and Dayan, 2014; Ziv, 2001), debris flows are associated with individual rain cells generated by active Red Sea troughs (e.g., Ahlborn et al., 2018; Ben David-Novak et al., 2004). ~~More rarely, subtropical jet stream disturbances can also generate flash floods (i.e., Tropical Plumes; Armon et al., 2018; Enzel et al., 2012; Tubi and Dayan, 2014; Ziv, 2001).~~ Thus, the deposition of alternating authigenic aragonite and detrital laminae, which dominate the record of Lake Lisan, the late Pleistocene predecessor of the Dead Sea (~70-14 ~~Kaka based on exposures~~; Begin et al., 1980; ~~although in the ICDP 5017 core there is evidence of earlier beginning of Lake Lisan; Neugebauer et al., 2016; Katz et al., 1977; Kaufman, 1971~~), throughout the majority of marine isotope stage 2 (MIS2) was attributed to annual deposition under seasonal climate during high lake levels and wetter-than-modern conditions, which sufficed to replenish the lake with necessary bicarbonate to support aragonite precipitation during summer and deliver detrital sediments during winter (Begin et al., 1980; Ben Dor et al., 2019; Haase-

Schramm et al., 2004), as was further confirmed by the comparison of laminae counting and radiometric dating (Prasad et al., 2004; Migowski et al., 2006). ~~In Lake Lisan~~ Similar to the modern hydroclimatic settings, winter inflow into Lake Lisan from its northern part was likely the dominant source of water and alkalinity, replenishing carbonate content in the carbonate-poor Dead Sea after aragonite precipitation took place during summer (Kolodny et al., 2005; Neev, 1963; Neev and Emery, 1967; Stein et al., 1997), whereas local floods in adjacent (ephemeral) streams delivered detrital sediments to the lake's depocenter (Nehorai et al., 2013).

Until recently, studies of the sedimentary record of the Dead Sea and its predecessors focused on available outcrops surrounding the lake (e.g., Bartov et al., 2003; Bartov et al., 2007; Stein et al., 1997; Prasad et al., 2004; Torfstein et al., 2008) as well as on short cores of Holocene sequences (e.g., Heim et al., 1997; Migowski et al., 2006). The broad aspect of their implications was thus limited due to local conditions and depositional hiatuses that form when lake levels fell below the outcrop's altitude (Machlus et al., 2000; Torfstein et al., 2013b; Torfstein et al., 2009) or by wave erosion during transgressive episodes of rising lake level. In addition, these outcrops were accumulated on the lake's shelf, and they therefore reflect its shallow-shallower environment, whereas the deeper part of the lake remained nearly inaccessible except for short coring campaigns (e.g., Garber et al., 1987; Nissenbaum et al., 1972). The recently collected ICDP-DSDDP cores from the lake's depocenter (ICDP site 5017) therefore provide a new regional perspective on sedimentary, limnological and hydrological processes in the lake (Fig. 1; e.g., Coianiz et al., 2019; Neugebauer et al., 2014). The 5017 cores of site 5017 were dated by combining ¹⁴C dating of macro organic debris including seeds and twigs (Neugebauer et al., 2014) with U-Th dating of primary aragonites (Torfstein et al., 2015), and by correlating their $\delta^{18}\text{O}$ with cave deposits (e.g., Lisiecki and Raymo, 2005; Bar-Matthews et al., 1999; Bar-Matthews et al., 2003). The age-depth model for the sections used in this study was established through a Markov chain Monte Carlo procedure utilizing ¹⁴C dates covering ~50 Kya (Fig. 2; Kitagawa et al., 2017).

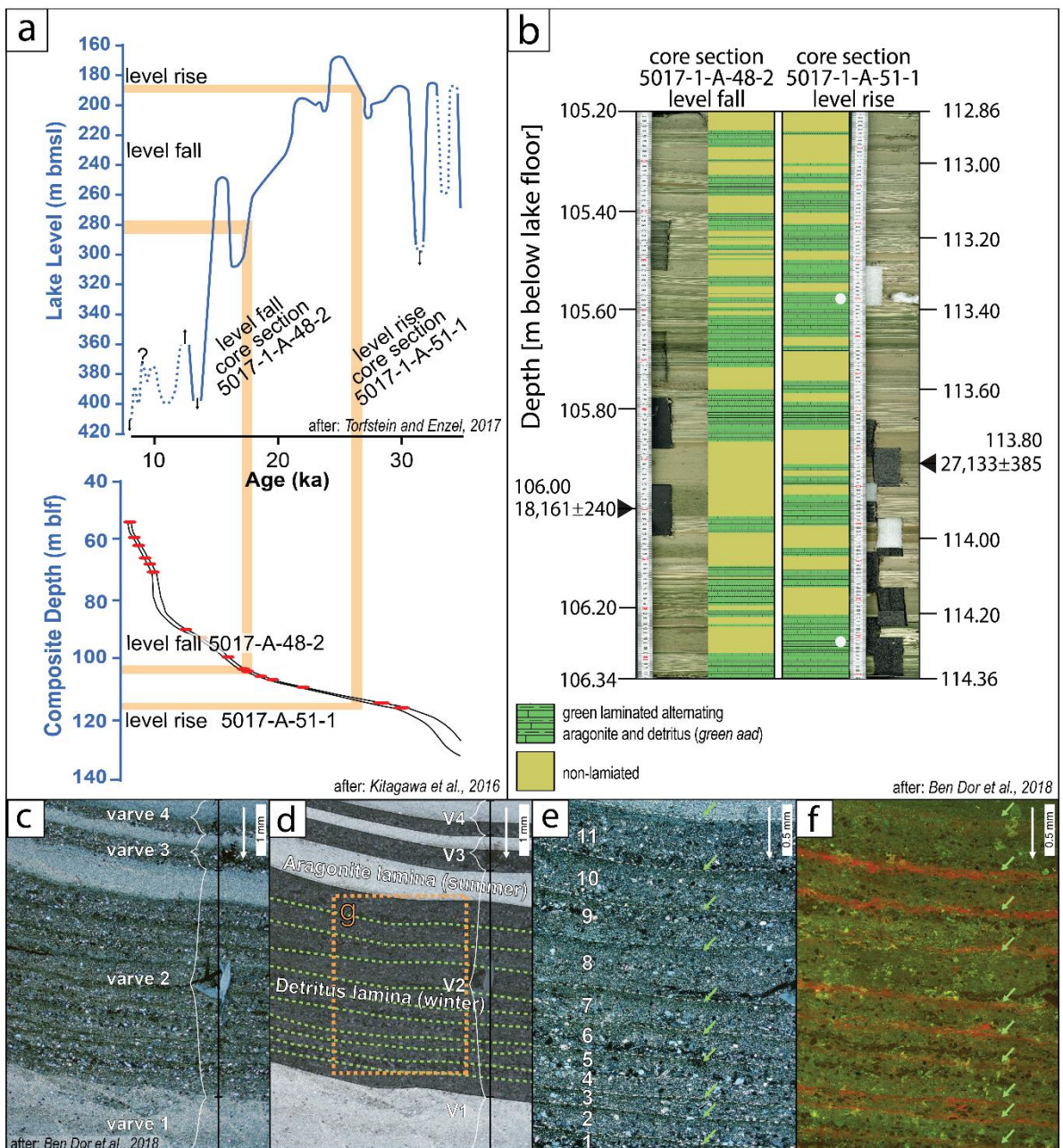
More recently, a detailed microfacies investigation revealed that the detrital laminae of the alternating aragonite and detritus facies are comprised of multiple sub-laminae, recording individual flooding events from adjacent streams that face the 5017 ICDP coring site 5017 (Ben Dor et al., 2018). Because the majority of these streams are ephemeral, and have relatively small watersheds (<1000 km²), such flash-floods may be triggered either by regional storms, that substantially contribute to the lake's annual water budget, and/or by smaller-scale local convection that has negligible impact on annual inflow. ~~small-scale local convective precipitation that has negligible impact on annual inflow. The alkalinity required to support annual aragonite precipitation cannot be supported by direct dust deposition (e.g., Ganor and Foner, 1996; Kalderon-Asael et al., 2009), whereas the dissolution and remobilization of accumulated dust from the watershed has the potential to supply bicarbonate that could increase inflow alkalinity (e.g., Crouvi et al., 2017; Belmaker et al., 2019). Although this cannot be resolved directly for MIS2, recent studies of denudation rates in the snow-affected Mt. Hermon (Avni et al., 2018) and the Judea region (Ryb et al., 2014), suggest that the dissolution of bedrock could not have increased alkalinity inflow by a factor greater than two, that would bear a more substantial impact on the northern part of the watershed. Thus the water and alkalinity budgets of the lake are ultimately dominated by rainfall over the northern part of the watershed (~75-85%), and subsurface inflow (~10-15%; Siebert et al., 2014; Levy et al., 2020), whereas contribution of floods to the water and (alkalinity) balance of the lake is negligible (5-10%; Armon et al., 2019).~~

The laminated sections of the ICDP-DSDDP core therefore provide a regional record of two (nearly) independent hydroclimatological variables at annual resolution: (a) the thickness of aragonite laminae (this study), and (b) the number of sub-laminae within detrital layers (Fig. 2; Ben Dor et al., 2018). Although more recent investigations indicate that aragonite laminae thickness is not linearly related to total annual inflow, as was previously suggested (Stein et al., 1997), it is correlated and monotonously associated with carbonate inflow and lake dilution of the lake, where increased inflow would result in

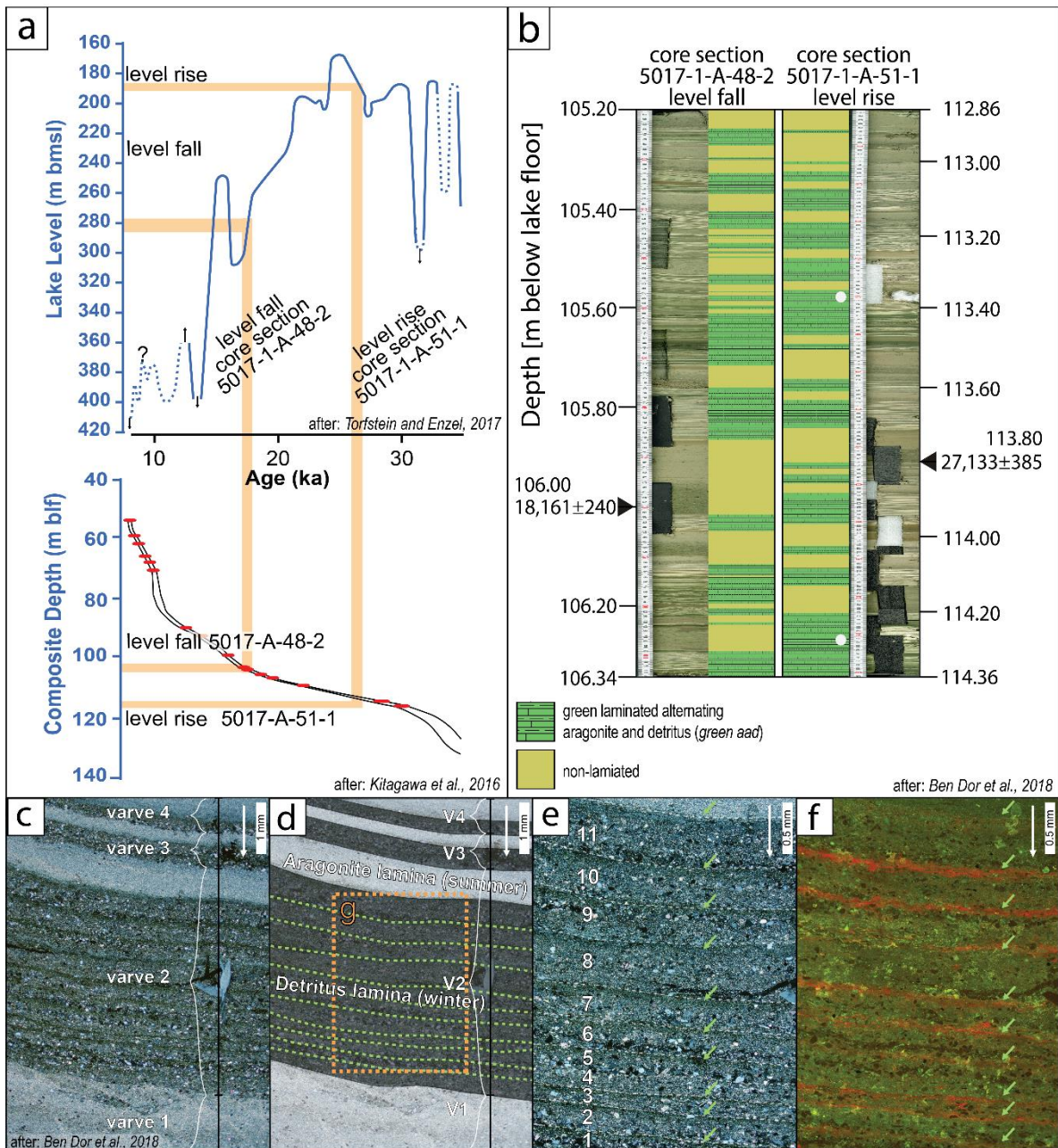
increased aragonite thickness, and may therefore ~~still~~ provide valuable insights on inherent ~~periodicities~~cyclicality and inter-annual inflow variability (Ben Dor et al., 2021).

200 The alkalinity required to support annual aragonite precipitation may be derived from dust settling directly on the lake and its watershed, as well as freshwater inflow. However, direct dust deposition is insufficient to support the deposition of aragonite laminae (e.g., Ganor and Foner, 1996; Kalderon-Asael et al., 2009), whereas the dissolution and remobilization of accumulated dust from the watershed, has the potential to supply bicarbonate that could increase inflow alkalinity (e.g., Crouvi et al., 2017; Belmaker et al., 2019). Although this cannot be directly addressed for MIS2, recent studies of the snow-affected Mt. Hermon region in Israel (Avni et al., 2018) and the denudation rates in the Judea region (Ryb et al., 2014), suggest that the dissolution of bedrock could not have increased alkalinity inflow by a factor greater than two, that would bear a more substantial impact on the northern part of the watershed. Thus the water and alkalinity budgets of the lake are ultimately dominated by rainfall over the northern part of the watershed (~75–85%), and subsurface inflow (~10–15%; Siebert et al., 2014; Levy et al., 2020), whereas the water (and alkalinity) contribution of floods is negligible (5–10%; Armon et al., 2019). Because the number of detrital sub-laminae, on the other hand, records the number of floods exceeding a threshold and reaching the coring site that deliver negligible water volumes (Ben Dor et al., 2018), the two series are addressed in this study independently in order to examine their properties and interactions. Thus, although floods over the small watersheds draining into the Dead Sea deliver both water and alkalinity into the Dead Sea (e.g., Belmaker et al., 2016; Golan et al., 2017), their overall negligible volume with respect to the annual inflow, makes the two studied proxies of aragonite thickness (this study) and the previously published number of detrital sub-laminae (Ben Dor et al., 2018) practically independent.

215



Because the number of detrital sub-laminae, on the other hand, records the number of floods exceeding a threshold and reaching the coring site (Ben Dor et al., 2018), the two series are addressed in this study independently in order to examine their properties and interactions.



225 Figure 2 - a) Top: Dead Sea lake level depicting the highest stage of Lake Lisan ~~during last glacial maximum~~, the Late Pleistocene predecessor of the Dead Sea, during last glacial maximum (Bartov et al., 2003; Torfstein and Enzel, 2017). Bottom: The age-depth model of the ICDP-DSDDP 5017-1 core and the position of the studied segments along the core (after Kitagawa et al., 2017). b) The studied sections of the ICDP-DSDDP cores dated to 18 ~~Kaka~~ and 27 ~~Kaka~~ (marine isotope stage; MIS2, ~15-30 ~~Kaka~~). c-f) Microscope images of alternating aragonite (summer precipitate) and detritus (deposited during winter) varves depicting a detrital laminae composed of multiple sub-laminae (labelled 1-11) deposited by individual floods (after Ben Dor et al., 2018).

230

3 Materials and methods

3.1 Microfacies analyses

Two chronologically-constrained segments (each ~1.5 meter long) ~~of the ICDP-DSDDP 5017-1 core deposited during 18~~ and 27 ~~Ka~~ were selected for this study (Fig. 2; Neugebauer et al., 2014). These segments are coeval with opposing climatic trends, reflected by independently-determined rising (27 ~~Kaka~~) and falling (18 ~~Kaka~~) lake level trends (Bartov et al., 2002; Torfstein and Enzel, 2017). The two sections were sampled continuously with overlap to prepare a sequence comprising 10-
 235 cm long ~~thin sections~~ thin-sections using a dry-freeze procedure adjusted for saline sediments (e.g., Brauer et al., 1999;

Neugebauer et al., 2015), and analyzed using a Hirox RH-2000 optical microscope (e.g., Ben Dor et al., 2018; Ben Dor et al., 2021). A total of ~700 varves (years) were counted and described in each segment. The segments comprise alternations of finely laminated varves (Ben Dor et al., 2019) and event-related deposits (Neugebauer et al., 2014)(ERDs; Neugebauer et al., 2014), attributed to debris flows (Ahlborn et al., 2018) and earthquakes (Fig. 2; Kagan et al., 2018). The nature of these sediments and ~~the way~~ their mode of formation ~~according, which is~~ based on the study of available exposures (Begin et al., 1980; Begin et al., 1974; Stein et al., 1997; Marco et al., 1996), and modern analogous lakes (e.g., Dean et al., 2015; Roeser et al., 2021), suggest that these detritus-aragonite couplets were deposited annually, thus forming varves. This is further supported by the uniformity of the sediments revealed by microfacies analyses carried out in this study, in which slight changes of sediment properties are observed in detail and the agreement between laminae counting and independent radiometric dating such as ¹⁴C and U-Th (Prasad et al., 2009; Haase-Schramm et al., 2004; Neugebauer et al., 2015). Because no deposition of alternating aragonite and detritus sedimentary facies takes place under modern conditions in the Dead Sea (e.g., Ben Dor et al., 2021), the interpretation of alternating aragonite and detritus facies as annual deposits is ~~a relatively solid assumption~~ used within the framework of this study, ~~as it cannot be directly determined for the studied interval Lake Lisan~~ (e.g., Prasad et al., 2004; Ben Dor et al., 2019; Ben Dor et al., 2020).

This study focuses on two properties of the varves interpreted as hydrological proxies: (a) the number of detrital sub-laminae in each detrital lamina, ~~reflecting the number of flooding events that reached the coring site~~ (Ben Dor et al., 2018), and (b) the thicknesses of aragonite laminae (this study). Because the thickness of detrital laminae (Fig. 2) is not directly linked to specific hydroclimatic processes, but instead depends on the interaction of multiple factors such as sediment availability and the geographical position of the activated catchment, it is not ~~analyzed here as a hydroclimatic proxy. The thickness of aragonite laminae was suggested to reflect annual inflow and lake dilution during the wet season (Kolodny et al., 2005; Stein et al., 1997), whereas individual sub laminae in detrital laminae correspond to flood events capable of delivering siliciclastic sediments to the coring site (Ben Dor et al., 2018). These sub laminae are attributed to floods that surpassed the threshold required to reach the coring site from their catchments.~~ ~~analyzed here as a hydroclimatic proxy. Missing data where laminae are trimmed or distorted (~5%) were imputed using singular spectrum analysis (e.g., Kondrashov and Ghil, 2006).~~

Because the typical number of sub-laminae is low, and the minimal number of detrital sub-laminae that can be counted is one, as no cases of “zero sub-laminae” are sedimentologically-distinguishable, varves comprising a single detrital lamina ~~should~~ ~~bear~~ considered as varves recording either years with no floods or years with a single flood. The two series deposited during rising and falling lake levels were compared using key statistical properties: the Mann-Whitney-Wilcoxon ranksum test to determine if they were sampled from two populations of a statistically different median (MWW; Mann and Whitney, 1947), and the Ansari-Bradley ranksum dispersion test (AB; Ansari and Bradley, 1960) to determine if they were characterized by statistically significant dispersion. Missing data where laminae are trimmed or distorted (~5%) were imputed using singular spectrum analysis (e.g., Kondrashov and Ghil, 2006).

3.2 Detecting intra-record regime shifts

A non-parametric test was developed in order to identify regime shifts as part of this study by comparing the observed running sum of sub-laminae count normalized by its mean ~~value~~ using consecutive multiple window widths ranging from 10 to 300 years, against ~~the~~ surrogate series generated by point-wise permutations of the data (Eq. 1; ~~Figs~~Fig. 3 and S1-S5).

$$\text{Eq. 1: } y_{w(i)} = \left\{ \begin{array}{l} i < \frac{w}{2} \\ \frac{w}{2} < i < N - \frac{w}{2} \\ i > N - \frac{w}{2} \end{array} \quad \frac{\sum n_j}{\widehat{y}_w}, \left[i - \frac{w}{2} \leq j \leq i + \frac{w}{2} \right] \right\}$$

- 280 **Equation 1 - the normalized running sum of sub-laminae counts.** $y_{w(i)}$ is the normalized running sum, i is the location index ranging between 1 and N , N is the number of data points in the studied series, $\sum n_j$ is the sum of sublaminae count over the range between $\left[i - \frac{w}{2} \leq j \leq i + \frac{w}{2} \right]$, w is the window width ranging from 10 to 300 by 10 years steps ($w = [10, 20, 30, \dots, 290, 300]$), and \widehat{y}_w is the mean normalized sum of n for window width w . The resulting $y_{w(i)}$ values larger than unity indicate flood-rich episodes, whereas $y_{w(i)}$ values lower than unity indicate flood-poor episodes.
- 285 Because the aim of this analysis is to assess the probability of observing decadal to centennial intervals of increased flood frequency (i.e., clustering of floods) whilst avoiding a-priori assumptions and parametrization, and because the two series ~~depicts~~ depict low serial dependence (Fig. S6), the surrogate time series were produced by point-wise permutations. After the running sum was normalized by its mean value for every window width, ~~and~~ local maxima values that are separated by at least half of the window width were considered for the analysis (Fig. 3c and 3d). The peaks were ranked in descending order and
- 290 compared against a dataset derived from 10,000 permutations without replacement of the respective series, revealing the significance level of observing intervals of the studied window width. Observed values larger than the 95th percentile of the permuted series are considered statistically significant ~~with a false positive error of at the~~ $\alpha=0.05$ confidence level (Fig. 3e and 3f). Because the significant peaks of different window widths overlap, the clusters were evaluated by considering their summed probabilities (Fig. 3g and 3h), and their edges were refined ~~by using the a~~ running MWW and AB tests, in which the
- 295 two halves of the window are compared against each other (Figs. S7-S8).

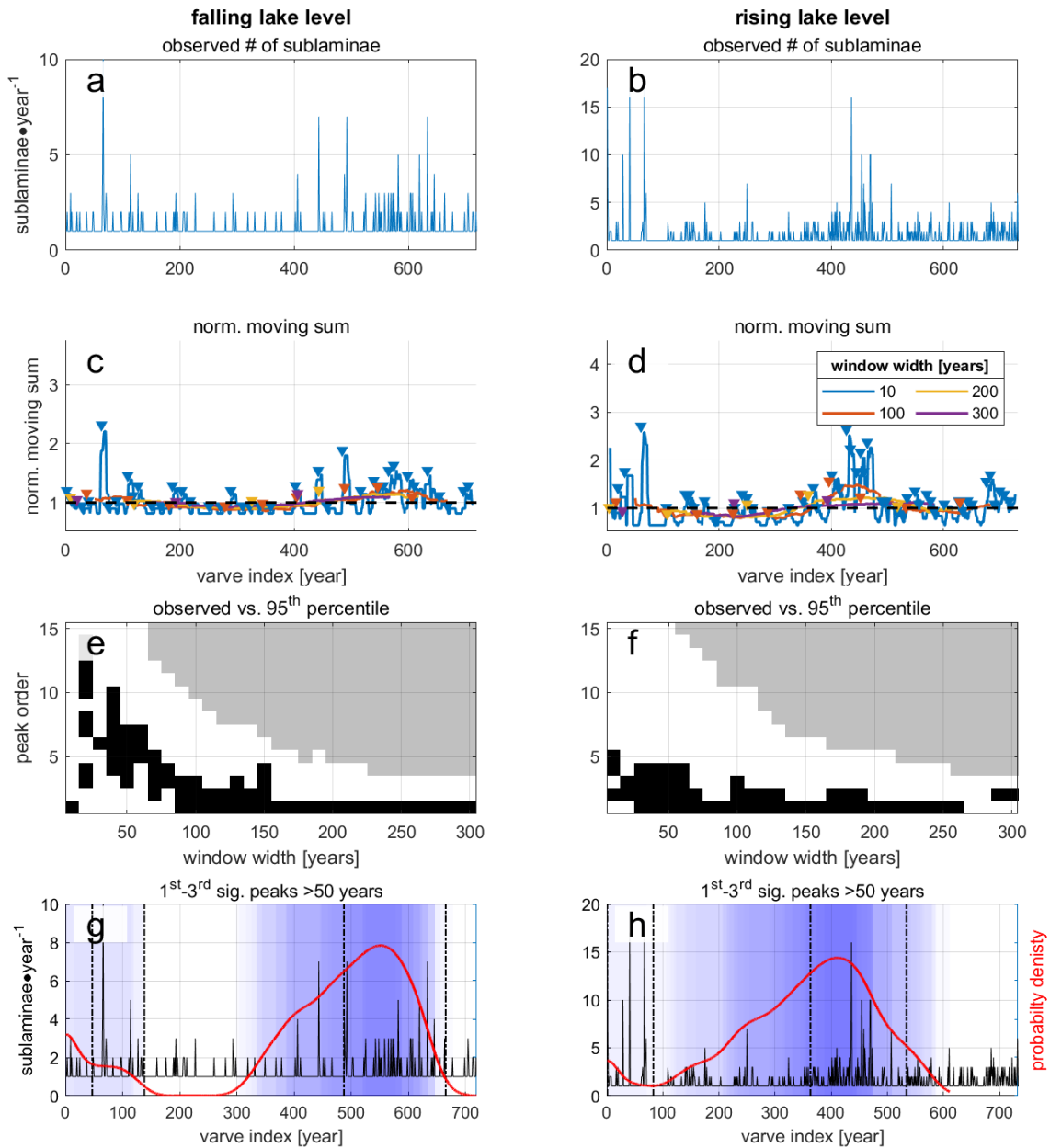


Figure 3: **results of the non-parametric test developed for identifying flood-rich episodes (i.e., flood clustering)** a,b) the studied series of flood frequency **analyzed/analysed** using microfacies analyses of two DSDDP core sections. c,d) the running normalized sum calculated for identifying flood clusters and its peaks (triangle) using different window widths. e,f) binary diagrams indicating where observed $y_{w(t)}$ values are higher than the calculated 95th percentile of the distributions derived from 10,000 randomly permuted series, and are thus statistically significant **at/considering** $\alpha=0.05$ (black pixels) or non-significant (white pixels). Missing values, where not enough peaks were detected to calculate the 95th percentile are **coded/colored** grey. g,h) the location of statistically significant peaks at $\alpha=0.05$ depicted as semi-transparent shading for the top three highly ranked peaks of window widths ranging between 50 and 300, **superimposed on the data series**. The red line depicts the probability of the summed identification of clusters by all window widths. The refined clusters are marked by dashed vertical lines.

Recurrence and joint-recurrence techniques and their analyses (*RQA* and *JRQA*) were applied to identify non-linear transitions and distinct regimes within the series (Eckmann et al., 1987). These methods can be used to detect abrupt transitions as well as short-term **periodic and cyclic or** oscillatory behaviours in non-stationary and noisy data by investigating their dynamics in the reconstructed phase space (Donges et al., 2011; Marwan et al., 2007). The following short introduction and **included the its** equations are based on the detailed review by Marwan et al. (2007), to which the keen reader is referred for further details.

The recurrence of the system is computed by considering the pairwise similarity (proximity) of points along its phase space trajectory reconstructed using a [selected](#) time delay (τ) and an embedding dimension (m). The recurrence plot (RP), which is used to efficiently visualize the recurrence of the studied series, is [generated/plotted](#) by calculating the $R_{i,j(\varepsilon)}$ matrix, through the binarization of the difference between the norm of the pairwise trajectories of steps in the reconstructed phase space using a predefined threshold ε (Eq. 2; Marwan et al., 2007). When the trajectory in two points (i and j) is smaller than ε , the value of the corresponding point ($R_{i,j(\varepsilon)}$) is set to [one/unity](#) in R , and the pixel painted black in the [RP-recurrence plot](#). Otherwise the value is set to zero and the corresponding pixel in the [RP-recurrence plot](#) is painted white.

$$\text{Eq. 2: } R_{i,j(\varepsilon)} = \theta(\varepsilon - \|\vec{x}_i - \vec{x}_j\|), \quad i, j = 1, 2, 3, \dots, N$$

Equation 2 (after Marwan et al., 2007) – the calculation of the recurrence matrix using a threshold ε , where N is the number of points of the reconstructed \vec{x}_i trajectory, and $\theta(\cdot)$ is the Heaviside function (step function), where $\theta(x) = 0$, if $x < 0$ and $\theta(x) = 1$ otherwise.

Similarly, the joint recurrence plot can be derived (JRP) for studying the dynamical relationship of two series or more [by/as](#) the product of [their](#) recurrence [plots/matrix](#) (Eq. 3; Romano et al., 2004).

$$\text{Eq. 3: } JR_{i,j(\varepsilon_{\vec{x}}, \varepsilon_{\vec{y}})} = \theta(\varepsilon_{\vec{x}} - \|\vec{x}_i - \vec{x}_j\|) \cdot \theta(\varepsilon_{\vec{y}} - \|\vec{y}_i - \vec{y}_j\|), \quad \vec{x}_i \in \mathbb{R}^m, \vec{y}_i \in \mathbb{R}^n, \quad i, j = 1, 2, 3, \dots, N$$

Equation 3 (after Marwan et al., 2007) – the calculation of the joint recurrence matrix as the product of two recurrence matrices calculated for two series with trajectories \vec{x} and \vec{y} , using the thresholds $\varepsilon_{\vec{x}}$ and $\varepsilon_{\vec{y}}$, respectively. N is the number of points of the trajectories, and $\theta(\cdot)$ is the Heaviside function (step function), where $\theta(x) = 0$, if $x < 0$ and $\theta(x) = 1$ otherwise.

The [RP-recurrence plot](#) of a [eye-like](#) system [characterized by cyclical components](#) would show diagonal lines parallel to the line of identity (LOI), which connects its lower left [corner with its and](#) upper right [one/corners](#), whereas a noisy system would be characterized by spotty and random appearance of points throughout the [RP-recurrence plot](#). Once the [RP-recurrence plot](#) is [calculated/established](#), its properties and the time dependent behaviour of the system can be studied by quantifying its recurrence using recurrence quantification analysis (RQA). [This is done](#) by computing different measures for each sub-matrix formed by sliding a square window along its LOI [with/by](#) a predefined [time](#) step. In this study the recurrence rate (RR), determinism (DET), the maximum length of a diagonal line within a sub-matrix (L_{max}) and the laminarity (LAM) metrics are used. The maxima of DET and L_{max} can be used to identify periodic-chaos and chaos-periodic transitions. Alongside those transitions [in, which are recorded as \$LAM\$ \(minima\), it is capable of identifying, \$LAM\$ could indicate](#) chaos-chaos transitions as well (maxima). The recurrence rate is the percentage of points in which recurrence occurs within the studied [section/segment](#) (Eq. 4).

$$\text{Eq. 4: } RR(\varepsilon) = \frac{1}{N^2} \sum_{i,j=1}^N R_{i,j}(\varepsilon)$$

The determinism (DET) reflects the extent to which the system maintains an ordered, cyclic and deterministic behaviour. Because uncorrelated, weakly correlated, stochastic or chaotic processes form very short [diagonals or none at all/diagonal lines \(if any\)](#), whereas deterministic processes generate longer [diagonals/diagonal lines](#), the ratio of recurrence points that form diagonal lines (with length $\geq l_{min}$) to all recurrence points can be used to estimate the main behaviour of the system within the studied [period/segment](#) (Eq. 5). In this study the minimal length of l (l_{min}), was set to $l_{min} = 2$.

$$\text{Eq. 5: } DET = \frac{\sum_{l=l_{min}}^N l P(l)}{\sum_{l=l}^N l P(l)}$$

Similar to DET , the laminarity (LAM) is computed as the portion of points forming [a-vertical line/lines](#) of minimal length v out of the entire set of recurrence points within the [RP-recurrence plot](#) (or in its sub-matrices).

$$\text{Eq. 6: } LAM = \frac{\sum_{v=v_{min}}^N v P(v)}{\sum_{v=1}^N v P(v)}$$

355 In order to decrease the influence of the tangential motion, LAM is computed using the points forming [vertical lines](#) (v) that exceed a minimal length v_{min} , which was set in this study [as to](#) $v_{min} = 2$. In cases where the [RPrecurrence plot](#) consists of more single recurrence points than vertical structures LAM will [decrease take low values](#).

360 [TheFinally, the](#) length of the longest diagonal line (L_{max}) is computed by identifying the longest diagonal line found within the [RPrecurrence plot](#) (or in its sub-matrices; Eq. 7).

$$\text{Eq. 7: } L_{max} = \max(\{l_i\}_{i=1}^{N_l})$$

where $N_l = \sum_{l \geq l_{min}} P(l)$ is the total number of diagonal lines.

365 This approach is specifically useful in this study because the studied proxies record the convolved non-linear interaction of climatic, hydrological and limnogeological processes, [and](#) because the effect of their interactions could stem from non-linear dynamics that bear very different implications on sedimentary sections (Marwan and Kurths, 2004; Marwan et al., 2003). The analysis was carried out using the CRP toolbox for MATLAB© after normalizing the series to zero mean and unit standard deviation (ver. 5.22; Marwan et al., 2007). The embedding dimension and the time-delay were determined using the false nearest neighbour approach (Kennel et al., 1992) and the mutual information method (Fig. S6; Marwan, 2011). The threshold ε was set to fit a recurrence rate (RR) of 0.1 using the max norm method (Schinkel et al., 2008), and the RQA (and JRQA) measures were calculated with a window of 30 years with a time step of a single year.

3.3 [Detecting periodic](#)Analysis of oscillatory components

375 Hydrological data are commonly skewed, and may exhibit short-term [periodic](#)behaviour that is difficult to identify using standard Fourier-derived approaches such as the periodogram (e.g., Blackman and Tukey, 1958; Welch, 1967). Wavelet analyses provide a set of [more](#) flexible ~~tool~~tools for identifying irregular and non-stationary [periodicities](#) in short time series (Lau and Weng, 1995; Torrence and Compo, 1998). The coherence of two series provides an [estimate](#)estimation of the importance of areas with high common power in the two series, that reflects the localized correlation coefficient in time-frequency space (Grinsted et al., 2004). Wavelet analyses were carried out using the Morlet wavelet function after normalizing the data to zero mean and unit standard deviation. The significance of the wavelet power and coherence were determined against red noise simulated using a lag-1 autoregressive process (AR(1)) using the cumulative area-wise approach for detecting false positive periodicities at the $\alpha=0.05$ [confidence level](#) (Schulte, 2019, 2016).

385 Singular spectrum analysis (SSA) is used to identify periodic and oscillatory [signals](#)components in short, non-stationary and noisy time series (Broomhead and King, 1986). Unlike wavelet and Fourier-based procedures, where the signal is compared against a predefined function, SSA identifies [principle](#)principal components that best explain the variance of the time-delayed series through the embedded matrix. This non-parametric approach reveals the dominant components that best explain the variance and defines their relative contribution [for generating](#)to the observed signal (Vautard and Ghil, 1989). This, in turn, allows the breaking-down of the signal into its principle components and calculating their corresponding reconstructed components (RCs), which demonstrate the extent [of contribution for to which](#) each component [contributes](#) to the signal (Ghil et al., 2002). Generally, SSA complements wavelet and other spectral analyses because it provides increased flexibility, and may identify oscillatory components of different [shapes](#)structures that change in time. Thus, the analyses of the individual RCs, and the determination of their dominant [periodic](#)cyclical components can point at dominant frequencies embedded [in within](#) the observed series, which in turn could stem from teleconnection patterns affecting hydroclimatic variability (e.g.,

NAO, SOI, etc.; [e.g., Feliks et al., 2010; Le Mouél et al., 2019; Seager et al., 2019](#)). In order to balance between the analyses
 395 complexity and usefulness, the SSA was performed with an embedding dimension (window) of ten years after visually
 inspecting the effect of the number of RCs on the relevant eigenvalues. The first RC (RC⁽¹⁾) was later used as the local trend
 component that was subtracted from the data as a high-pass filter to reveal short-term ~~periodicities~~[cyclicities](#) (Fig. S9). The
 SSA RCs were additionally ~~analyzed~~[analysed](#) using the Welch periodogram for evaluating the RCs power spectral density
 (Welch, 1967), and wavelet analyses ~~using together with~~ the area-wise ~~test for~~ significance ~~test~~ (Schulte, 2016, 2019) in order
 400 to compare their time-frequency properties during [the identified](#) cluster and background periods. The Welch periodogram was
 calculated ~~after applying a Hamming window of width 25 years and an overlap of 50%, applied to merge close periodic~~
~~components and reduce spectral noise~~, after subtracting the mean from the series and zero-padding it to 2¹¹ points in order to
 minimize spectral leakage (~~Figs. and applying a Hamming window of 25 years width and an overlap of 50%, in order to merge~~
[close periodic components and reduce spectral noise \(Figs. S10-S13\)](#)).

405 4 Results

4.1 Microfacies analyses

The studied segments are dominated by greenish alternating laminae of aragonite and detritus (Fig. 2), ~~and are~~ characterized
 by a typical laminae thickness of <1 mm. Detrital laminae are dominated by [clay with quartz](#), ~~clay~~ and organic matter, with
 some calcite, dolomite and feldspar grains, commonly showing graded bedding, a clay cap ~~of~~ and a thin lamina of amorphous
 410 organic matter (Fig. 2). The laminated segments are interrupted by massive or graded [event related deposits \(ERDs\)](#) attributed
 to abrupt mass wasting events (e.g., ~~turbidites~~[turbidites](#) and slumps), triggered by earthquakes (Kagan et al., 2018), debris
 flows and slope instability (Ahlborn et al., 2018). Both laminae thickness and number of sub-laminae show statistically
 significant larger mean and variance during lake-level rise (~~←27 Ka~~) than during lake-level fall (~~←18 Ka~~; ~~Table~~[\(Tables 1 and](#)
[2](#); Figs. 4 and 5).

415 Aragonite laminae thicknesses range between 51 and 2,259 μm (μ=457μm, σ=308 μm), and 53 and 6,020 μm (μ=642 μm,
 σ=529 μm) ~~in the falling~~[during lake-level fall](#) and ~~rising segments~~[rise](#), respectively. Detrital laminae thicknesses range from
 27 to 13,136 μm (μ=312μm σ=638 μm), and 27 and 8,760 μm (μ=416 μm, σ=675 μm) in the falling and rising segments,
 respectively. The number of sub-laminae during the falling lake level ranges between 1 and 10 (μ=1.2, σ=0.7), and between 1
 420 and 17 (μ=1.6, σ=1.6) ~~in the~~[during](#) rising lake level, ~~respectively~~ (Table 1). The MWW test indicates a significant difference
 between all studied proxies when comparing the two studied series (p value <<0.05). The difference in dispersions of all
 variables between rising and falling lake levels are statistically significant [using the Ansari-Bradley test](#) (p value<<0.05) except
 for detrital laminae, ~~where the Ansari Bradley test failed to reject the null hypothesis~~ (p value≈0.12; [Table 2](#)). All three
 425 parameters show positive skewness of 2.1 ~~μm~~ and 3.5 ~~μm~~ for aragonite laminae thickness, 12.7 ~~μm~~ and 7.6 ~~μm~~ for detrital
 aragonite laminae, and 5.9 and 6.1 of sublaminae count during falling and rising lake levels, respectively. No significant
 correlation exists between any two of the parameters in each time series, with the exception of a moderate correlation between
 the number of sub-laminae in the detrital laminae and [detrital](#) laminae thickness (Fig. 4; r=0.52 and 0.61, for falling and rising
 lake levels, respectively; with p values <<0.005).

430

Table 1 – Bulk statistical properties of the studied sedimentary series.

Rise/fall	Parameter	Unit	Min	Max	Median	Mean	Std. deviation	Skewness
-----------	-----------	------	-----	-----	--------	------	-------------------	----------

fall	aragonite	µm	51	2,259	389	458	308	2.1
fall	detritus	µm	27	13,136	167	316	639	12.6
fall	number of detrital sub-laminae	count	1	10	1.0	1.2	0.7	5.9
rise	aragonite	µm	53	6,020	512	643	529	3.5
rise	detritus	µm	27	8,760	261	416	675	7.6
rise	number of detrital sub-laminae	count	1	17	1.0	1.6	1.6	6.1

Table 2 – p values of the statistical comparison between the bulk studied series

Parameter	Test ¹	p value ²	Significant at $\alpha=0.05$
aragonite	MWW	< 0.001	yes
detritus	MWW	< 0.001	yes
number of detrital sub-laminae	MWW	< 0.001	yes
aragonite	AB	0.001	yes
detritus	AB	0.248	no
number of detrital sub-laminae	AB	< 0.001	yes

1 – MWW – Mann-Whitney-Wilcoxon ranksum test, AB – Ansari-Bradley dispersion test.

435 2 – tests with p values smaller than 0.05, are considered significant at $\alpha=0.05$.

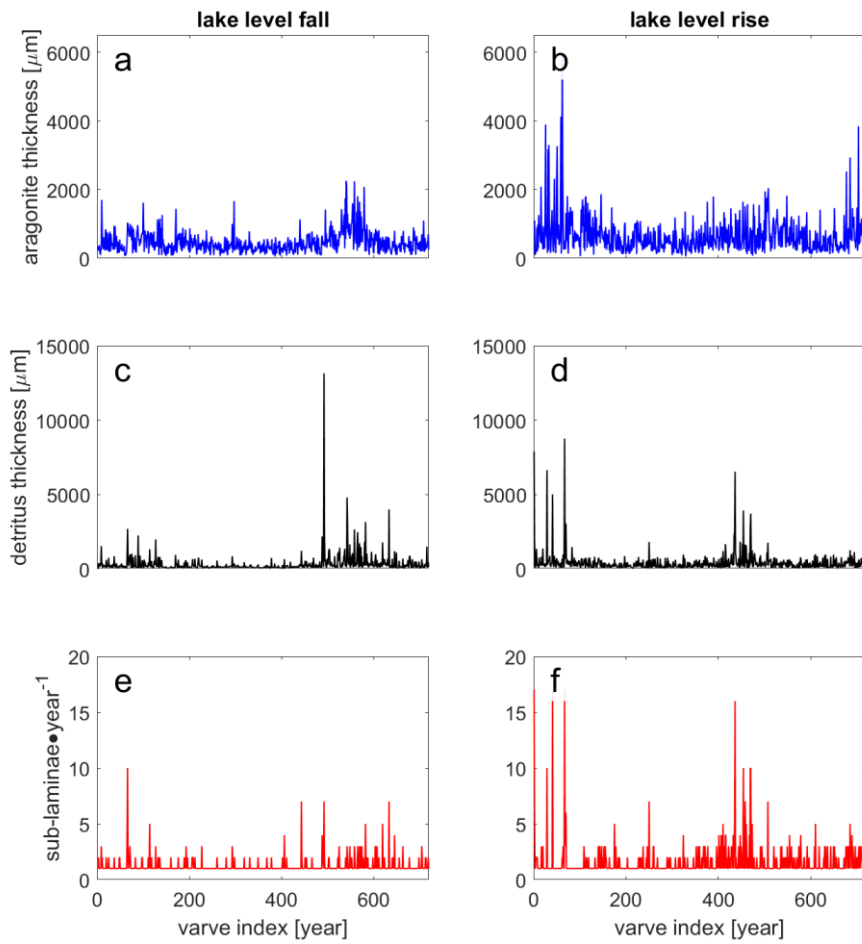
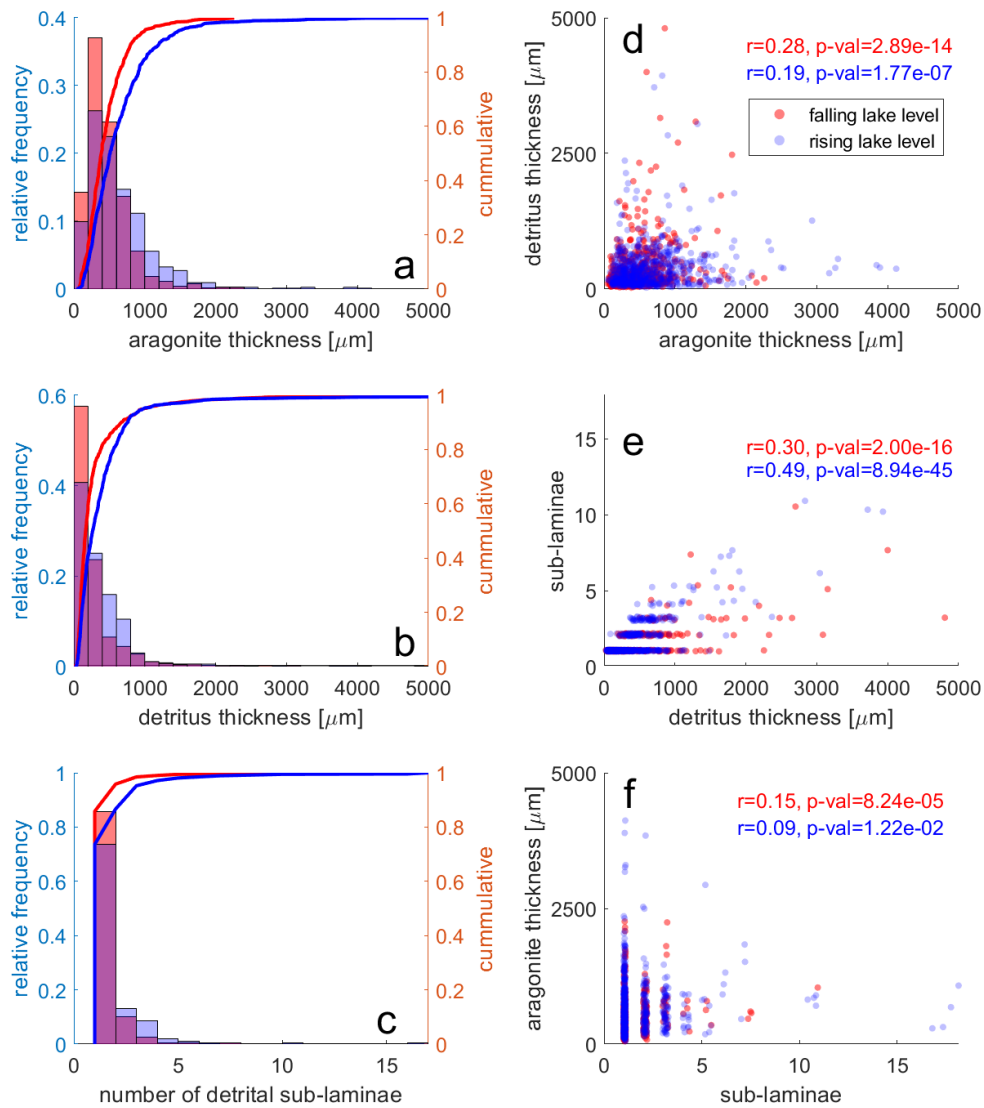


Figure 4 – Time series of microfacies analysis of the studied varved sections. (a, b; blue) aragonite laminae thickness, (c, d; black) ~~detritus~~detrital laminae thickness, (e, f; red) number of detrital sub-laminae.



440

Figure 5 – Distributions and scatter plots of the trivariate geological time series showing the distributions of (a) aragonite laminae thickness, (b) detritus laminae thickness and (c) number of sub-laminae counted in each detrital lamina. Plots d-f show the correlations between aragonite and detritus thickness (d, $r^2=0.07$, 0.03), number of floods and detritus thickness (e, $r^2=0.27$, 0.37), and number of floods and aragonite laminae thickness (f, $r^2=0.03$, 0.01)

445

4.2 Detecting intra-record regime shifts

Two clusters of intense flood frequency were identified in each of the studied series (Fig. 3; Table 3). ~~Although two clusters are identified, However~~ one of the two clusters in each series appears more robust in comparison with the other, as it was identified using multiple window widths (Figs. S5), and the clusters are labelled as robust and less robust accordingly (Table 3). However, it is noted that this different robustness estimation could stem from an “edge effect” bias, ~~that~~which limits the analysis of segments close to the edges of the series when large window widths are applied. The RPs~~recurrence plots~~ of aragonite series depict some short diagonal lines, whereas those of the sub-laminae show more spotty properties with blocky character (Figs. 6 and 7). An increase in both *DET* and *L_{max}* is identified close to ~~the clusters’~~edges of clusters, although the RQA measures fluctuate throughout the series, and do not exhibit pronounced changes or trends with respect to the identified

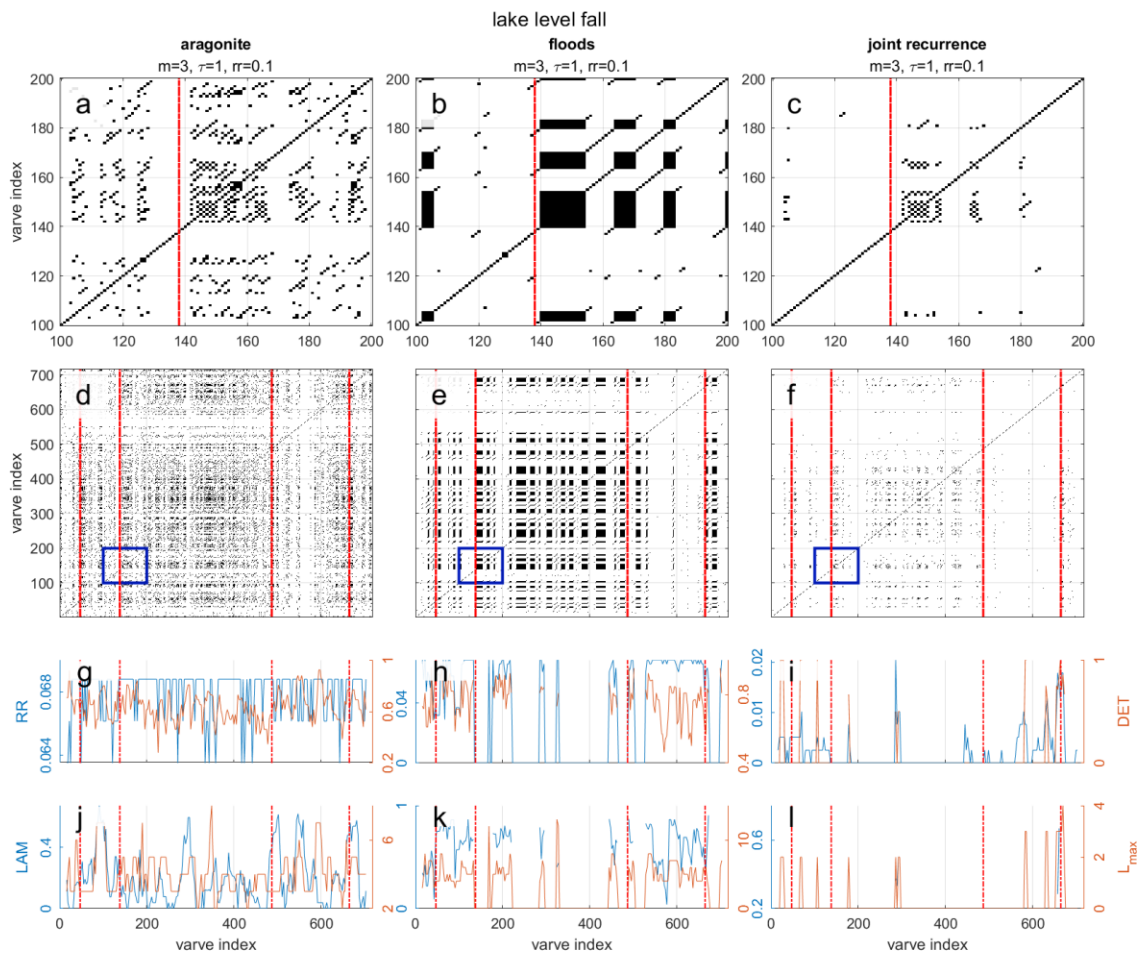
450

455 clusters. Both JRPs depict fairly low recurrence with spotty and patchy patterns, with some diagonal lines in the series of the falling lake level.

Table 3 – Identified clusters in the two studied series following the procedure [Appendix B based on](#) [described in section 3.2 using the number of detrital sub-laminae.](#)

	Level fall [index years]	Estimated robustness	Level rise [index years]	Estimated robustness
1 st cluster	47-138	Less robust	1-83	Less robust
2 nd cluster	487-662	Robust	363-534	Robust

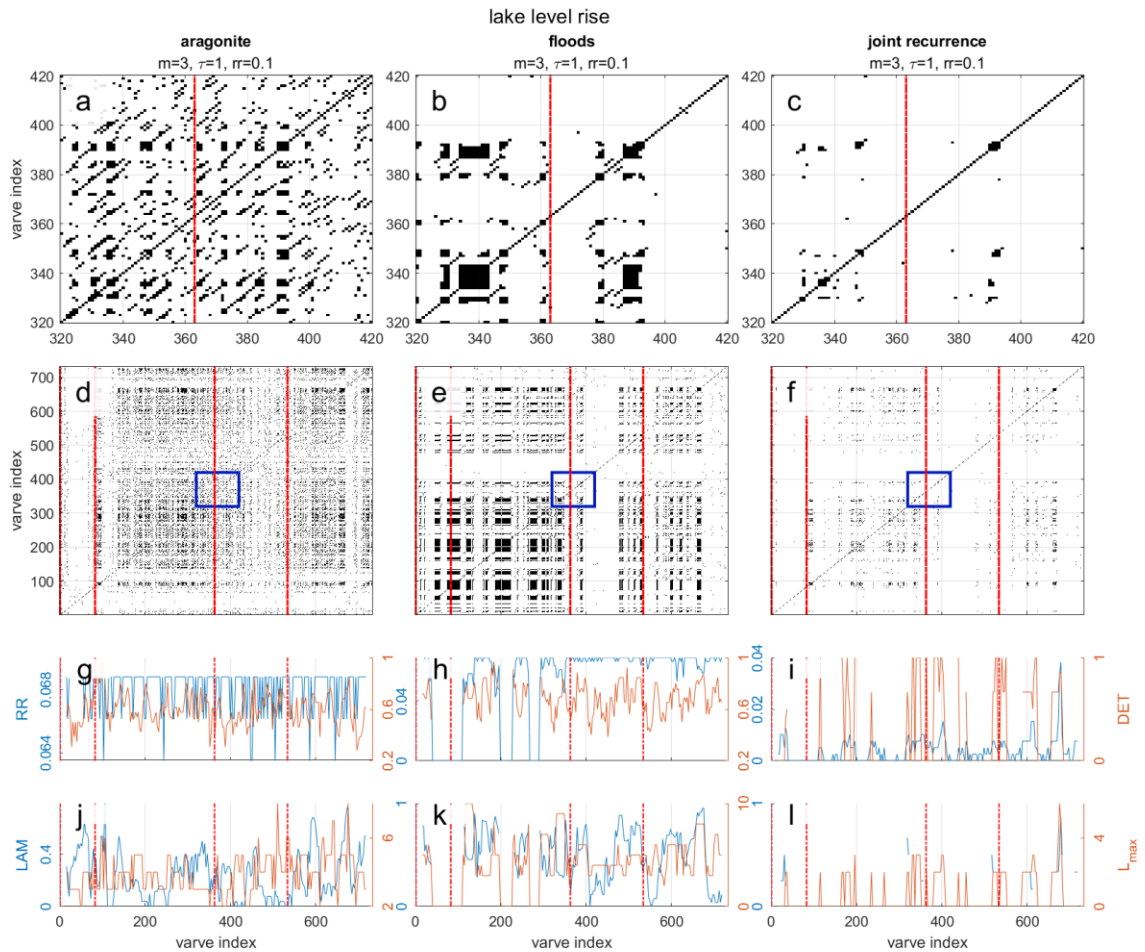
460



465

470

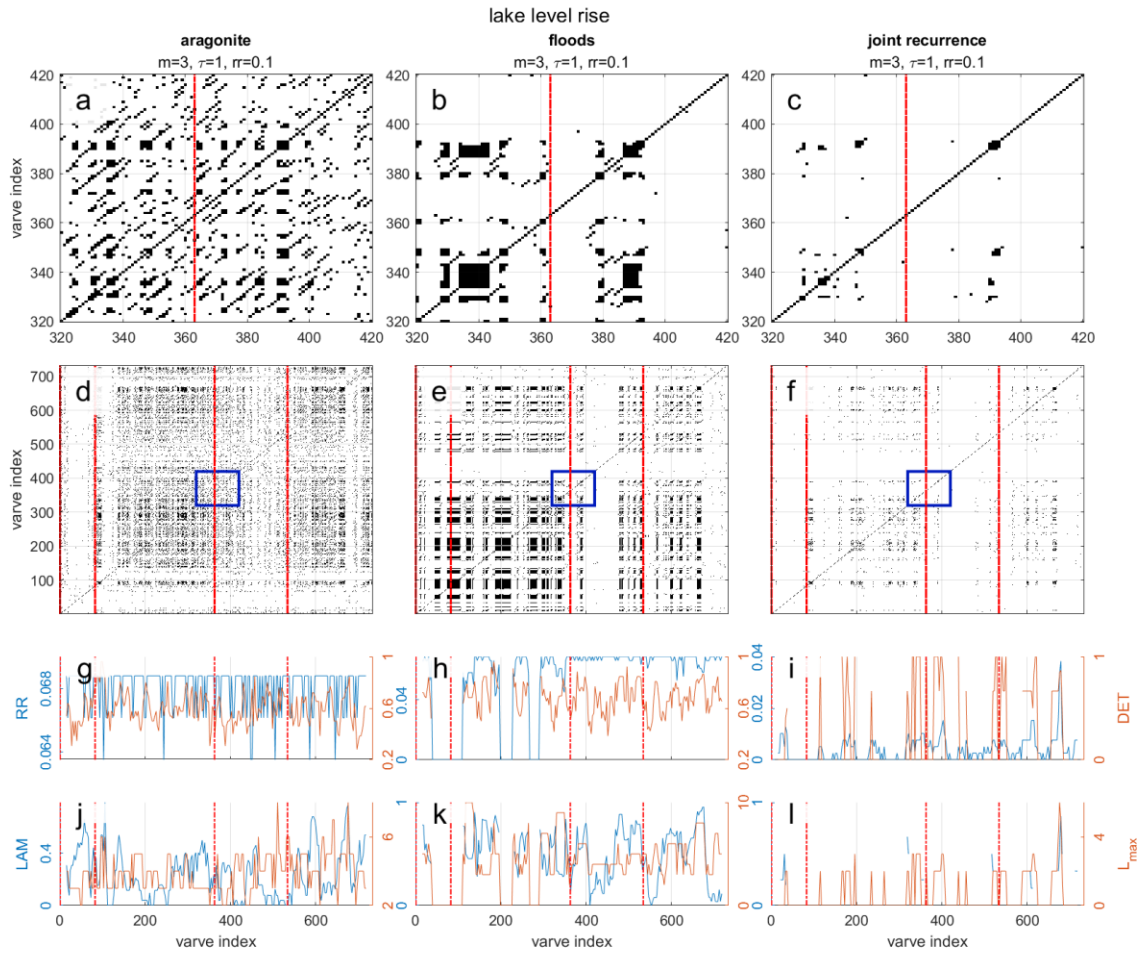
Figure 6 – (a-c) Enlarged segments of the recurrence plots of the studied lake-level fall for aragonite thickness (a), flood frequency (b) and the joint recurrence plot for the two proxies (c). (d-f) Recurrence plots of the aragonite thickness (d), flood frequency (e) and the joint recurrence plot for the two proxies (f), with blue rectangles indicating the extent of data presented in (a-c). Note the parallel diagonal lines that characterize the aragonite thickness series (a,d), and point on an inherent oscillatory behaviour, whereas the flood series (b,e) forms sporadic points and polygons that reflect a more chaotic or random behaviour. (g-i) The recurrence rate (RR) and the determinism (DET) coefficient using a running window size of 30 years and a single year step for aragonite thickness (g), floods (h) and the joint recurrence (i). (j-l) The laminarity (LAM) and the maximum length of the diagonal line within the sub-matrix (L_{max}) coefficient using a running window size of 30 years and a single year step for aragonite thickness (j), floods (k) and the joint recurrence (l). The analyses were performed after detrending the data by subtracting the $RC^{(1)}$ of the SSA, and normalizing to zero mean and unit standard deviation. The selected parameters for the embedding are m (dimension), τ (delay) and ϵ (threshold) used for space phase reconstructions are depicted in the figure. Red lines represent possible clusters identified independently of the recurrence analyses.



(a,d), and point on to Figure 7 – (a-c) Enlarged segments of the recurrence plots of the studied lake-level rise for aragonite thickness (a), flood frequency (b) and the joint recurrence plot for the two proxies (c). (d-f) Recurrence plots of the aragonite thickness (d), flood frequency (e) and the joint recurrence plot for the two proxies (f), with blue rectangles indicating the extent of data presented in (a-c). Note the parallel diagonal lines that characterize the aragonite thickness series (a,d), and point on an inherent oscillatory behaviour, whereas the flood series (b,e) forms sporadic points and polygons that reflect a more ~~chaotic~~ **chaotic** or random ~~behaviour~~ **behaviour**. (g-i) The recurrence rate (*RR*) and the determinism (*DET*) coefficient using a running window size of 30 years and a single year step for aragonite thickness (g), floods (h) and the joint recurrence (i). (j-l) The laminarity (*LAM*) and the maximum length of the diagonal line within the sub-matrix (*L_{max}*) coefficient using a running window size of 30 years and a single year step for aragonite thickness (j), floods (k) and the joint recurrence (l). The analyses were carried over after detrending the data using the SSA $RC^{(+)}$. Selected parameters for the embedding are *m* (dimension), τ (delay) and ϵ (threshold) used for space phase reconstructions are presented in the figure. Red lines represent possible clusters identified independently of the recurrence analyses.

480

485



490 **Figure 7**—(a-c) Enlarged segments of the recurrence plots of the studied lake level rise for aragonite thickness (a), flood frequency (b) and the joint recurrence plot for the two proxies (c). (d-f) Recurrence plots of the aragonite thickness (d), flood frequency (e) and the joint recurrence plot for the two proxies (f), with blue rectangles indicating the extent of data presented in (a-c). Note the parallel diagonal lines that characterize the aragonite thickness (a,d), and point on to an inherent oscillatory behaviour, whereas the flood series (b,e) forms sporadic points and polygons that reflect a more chaotic or random behaviour. (g-i) The recurrence rate (RR) and the determinism (DET) coefficient using a running window size of 30 years and a single year step for aragonite thickness (g), floods (h) and the joint recurrence (i). (j-l) The laminarity (LAM) and the maximum length of the diagonal line within the sub-matrix (L_{max}) coefficient using a running window size of 30 years and a single year step for aragonite thickness (j), floods (k) and the joint recurrence (l). The analyses were carried over performed after detrending the data using by subtracting the $RC^{(1)}$ of the SSA- $RC^{(4)}$. Selected, and normalizing to zero mean and unit standard deviation. The selected parameters for the embedding are m (dimension), τ (delay) and ϵ (threshold) used for space phase reconstructions are presented depicted in the figure. Red lines represent possible clusters identified independently of the recurrence analyses.

4.2 Detecting periodic components

Recurrence analyses3 Analysis of aragonite thicknesses indicate periodic or oscillatory behaviours, reflected by the components

505 The appearance of short diagonal lines in the recurrence plot of the aragonite thickness series indicates either intermittent periodic or weakly to moderately chaotic behaviours (Figs. 6 and 7). Conversely, the flood frequency series present blocky and irregular patterns that indicate an underlying chaotic, random, or practically non-periodic process (Figs. 6 and 7). In particular, the segments identified as clusters demonstrate some abrupt changes in the studied RQA measures that could indicate a shift in the system's dynamics, both in aragonite thickness and in the number of sub-laminae. Although this behaviour is somewhat expected for the sub-laminae series that was used to determine clusters in the first place, it is also evident for the aragonite series.

Discontinuous short-term patches of increased spectral power of periodicities of the annual-decadal band time scales appear sporadically throughout the entire dataset in both aragonite and flood frequency series (Fig. 8). However, these short-term oscillations/periodic components are not significant with an $\alpha=0.05$ confidence level, and additionally do not pass the global significance test. Instead, a couple of the significant patches that appear within this spectral band appear within clusters as vertically stretched vertical patches that range stretch over a set range of periodicities ranging time scales from sub-decadal to a multidecadal/multi-decadal (30-60 years) frequency bands, which indicate that these periodicities are the elevated spectral power in those frequency bands can be attributed to the abrupt pulse of increased variance occurring during the identified clusters (Hochman et al., 2019). These several (e.g., Hochman et al., 2019). Nevertheless, several of these significant patches pass the global significance test after detrending using the RC⁽¹⁾ of the SSA (Fig. S14). A high spectral power in the centennial- to bicentennial band (~120-250 years) periodic component is observed in both series of aragonite thickness series/thicknesses, although its significance cannot be determined as it falls largely outside the cone of influence, and it fails the cumulative area-wise significance test. A similar periodic/cyclical component is also identified in the sub-laminae series during lake-level rise, but not in the interval of lake-level fall. Altogether, the wavelet analyses do not suggest a robust detection of periodic/cyclical components in any of the studied series.

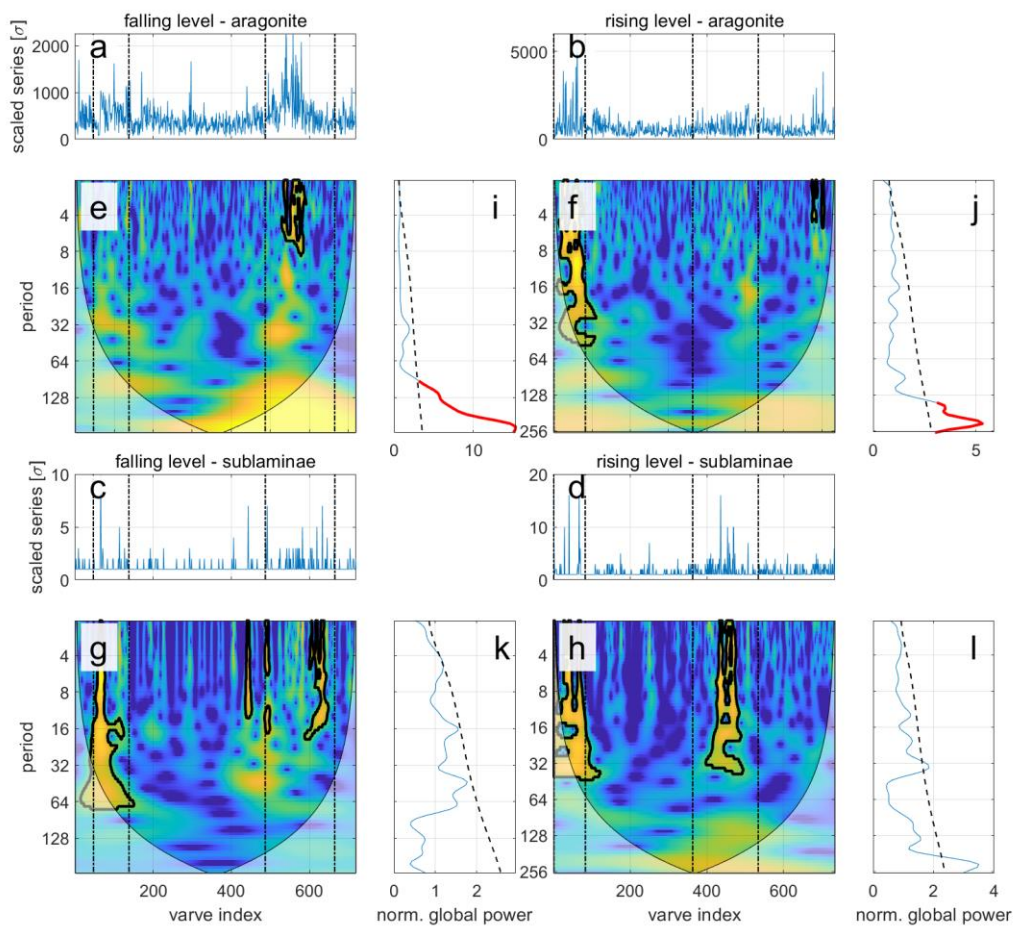


Figure 8 – Wavelet and global-wavelet spectrogram of aragonite thickness and flood frequency during falling (left) and rising (right) episodes. Periodicities/Patches with significance level above 0.95 ($\alpha=0.05$) of detected using the cumulative area-wise significance test are depicted by a bold black line (Schulte et al., 2018; Schulte, 2016). Each triplot section shows the normalized data (a-d), the wavelet spectra (e-h) and the global wavelet spectra (blue) compared against the significance test of the global wavelet power spectra (dashed black, i-l). Significant peaks of arcs are marked in red (Schulte, 2019). Vertical dashed vertical lines in (e-h) depict clusters identified as episodes of increased flood frequency. Note that the short-term periodic/cyclical component in the global wavelet spectra, which fail the significance of test using the original series, are found to be significant in the analysis of the detrended series (Fig. S14).

The SSA RCs are characterized by several ~~periodic~~ components (Figs. S10-S13). The first two components are considered as the local trend component, and accordingly depict persistent “long-wave” ~~periodic~~ components ~~with wave lengths characterized by a time scale of~~ >32 years. The ~~following~~ components ~~show~~ roughly ~~show~~ three peaks characterized by ~~periodic~~ components of sub-decadal frequencies.

5 Discussion

5.1 The mechanistic link between mean properties and variability

The poor correlation between aragonite thickness and the number of sub-laminae testifies to their low inter-dependence, and strengthen their interpretation as (nearly) independent proxies of the hydrological cycle in the Dead Sea watershed, ~~which is~~ in accordance with the previous interpretation of their ~~roles in relationship with~~ the hydrological cycle (Ben Dor et al., 2021; Ben Dor et al., 2018). Because of the unique hydroclimatic settings of the lake and its sedimentary record, ~~the record~~ cannot be directly interpreted ~~from the perspective of using a standard~~ a flood frequency analysis (e.g., Metzger et al., 2020), where the frequency and magnitude of floods in individual watersheds ~~is analyzed. This is because are studied. Indeed, the~~ detrital sub-laminae in the ICDP-DSDDP core ~~record~~ capture the number of flooding events, ~~which~~ potentially ~~last~~ lasting up to several days (Nehorai et al., 2013), ~~that~~ which exceeded the threshold required to reach the coring site at the lake depocenter (Ben Dor et al., 2018), instead of recording discharge properties at individual watersheds. Furthermore, the bathymetry of the basin dictates that only large-enough floods in tributaries situated ~~on both escarpments~~ in front of the coring site ~~on both sides of the escarpment~~, could have deposited detrital material at the coring site (Fig. 1). Although this aspect masks some of the delicate features that could have been otherwise extracted such as in the analyses of modern measurements, its length and established context with respect to regional climatic conditions ~~testifies to~~ demonstrates its value for interpreting hydroclimatic variability during episodes of climate change.

Available modern observations of sediment and water transport-paths into the lake, cannot unambiguously determine which synoptic systems affected the eastern Mediterranean ~~Sea~~ when the studied sediment segments were deposited during the ~~last glacial maximum (LGM-)~~. Nevertheless, considering available data that addresses this question, the likely suggestion that dominant weather regimes and synoptic circulation patterns during the LGM were similar to present is adopted for the sake of discussion in the framework of this work (e.g., Greenbaum et al., 2006; Amit et al., 2011; Enzel et al., 2008), with some possible modifications of their spatial properties (e.g., Goldsmith et al., 2017; Keinan et al., 2019). By considering that the dominant synoptic-scale circulation patterns during the late Pleistocene resemble modern observations in the region (Enzel et al., 2008), it can be argued that flooding ~~events~~, recorded as detrital sub-laminae at the depocenter of Lake Lisan, can be attributed to ~~any of~~ the three key synoptic patterns that govern precipitation over the eastern Mediterranean ~~Sea and southern Levant~~ (e.g., Armon et al., 2019). It is further suggested that the interplay and relative frequency of these three systems determine mean climatic conditions, ~~that determine which, in turn, determines~~ the Dead Sea lake level and ultimately propagate into its sedimentary record (~~Weber Torfstein et al., 2021; Waldmann 2015; Neugebauer et al., 2017 2014~~). Thus, the association of increased flood frequency with rising lake levels was interpreted as reflecting increased frequency and/or modulation of the Mediterranean Lows characteristics that deliver the majority of annual precipitation ~~over the Dead Sea watershed, and hence determine annual inflow into the lake (Saaroni et al., 2010) to the Dead Sea watershed, and hence determine annual inflow into the lake (Saaroni et al., 2010; Enzel et al., 2008; Armon et al., 2019)~~. However, a more detailed comparison of flood frequency with aragonite laminae thickness, that reflects annual inflow into the lake and the dilution of its epilimnion (Kolodny et al., 2005; Stein et al., 1997; Ben Dor et al., 2021), reveals more subtle insights and a delicate interplay of hydroclimatic factors manifested through the watershed during opposing climatic regimes.

Both aragonite laminae thickness and flood frequency have larger mean and variance during lake-level rise (Table 1). Because rising lake levels indicate a “wetter-an on-average” wetter climate, this relationship between mean and variance is similar to that observed in modern hydrologic parameters such as precipitation (e.g., Morin et al., 2019). The observed relationship between the two studied proxiesproperties, thus, strengthens the interpretation of these sedimentary proxies as hydroclimatic proxies. Namely, the increased thickness of aragonite laminae and the increased number of detrital sub-laminae suggests that the episodes of rising lake level were characterized by both-by increased annual inflow and increased flood frequency. As suggestions invoking increased-The ongoing debate on the effects of climate change on flood frequency were raised both forresulted in approaches suggesting that increased frequency of floods is coupled with drying of the eastern Mediterranean or with wetter and drierclimatic conditions were made (e.g., Alpert et al., 2002; Rohling, 2013; Yosef et al., 2019), this observation demonstrates. The results presented here suggest that increased flood frequency of floods duringis likely coupled with wetter intervals rather than with dryer conditions in the eastern Mediterranean climate zones is the likely scenario. Furthermore, the observed coupling of increased thickness of aragonite laminae with increased flood frequency may support their formation by a common hydroclimatic mechanism, such as i.e., the increased occurrence of Mediterranean low-pressure systemsLows (Armon et al., 2019; Enzel et al., 2008; Ben Dor et al., 2018; Goldreich et al., 2004).

5.3 Periodic2 Oscillatory components and hydroclimatological pacing

One of the goals in studying hydroclimatological proxies is identifying key periodicicyclical components that pace short-term variability under different mean climatic regimes (e.g., Ghil et al., 2002; Grinsted et al., 2004). Because (a) the thickness of aragonite laminae was suggested to reflect hydroclimatic (Kolodny et al., 2005) and limnologic conditions (Ben Dor et al., 2021), and (b) periodicitiescyclical behaviour attributed to solar cycles were previously identified by spectral analyses of laminae thickness at the exposed coeval White Cliff Member outeropof the Lisan Formation at Masada deposited during MIS2 (Prasad et al., 2004), a similar attempt was made in this study to identify similar periodicicyclical components as well. Although Prasad et al., (2004) report periodicitiesreported cyclical components of 50-60 years, the increased power observed in these spectral bands was not found to be significant in the studied sections at the $\alpha=0.05$ confidence level (Fig. 8; Schulte, 2016, 2019).

The North Atlantic oscillation (NAO) and the Eastern Atlantic (EA) patterns were suggested to affect interannual precipitation variability over the eastern Mediterranean Sea (e.g., Feldstein and Dayan, 2008; Feliks et al., 2010; Krichak et al., 2002; Seager et al., 2019), primarily due to their reported effect on discrete precipitation-bearing synoptic patterns over the eastern Mediterranean (e.g., Black, 2012). Other studies, on the other hand, have suggested that unlike in western Turkey, NAO shows only minimal direct impact on precipitation in the Levant, and that it might affect temperature instead (Enzel et al., 2003; Seager et al., 2020; Ziv et al., 2006). similar to these Although such relationships are hard to identify in geological records, a North Atlantic impact over the Dead Sea hydrology during the last glacial was identified here (Figs. 8, S14)-by lake-level reconstructions, where abrupt lake-level drops took place during Heinrich events (Bartov et al., 2003). Additionally, a cyclical component of a sub-decadal to decadal frequency bands (4-5, 7-8 and ~11 years), which were attributed to NAO, was also identified in laminated halite sequences deposited during the last interglacial (Palchan et al., 2017). These authors interpreted the cyclicity based on modern observations, which indicate that such pacing may manifest temperature variations, rather than precipitation, as temperature seasonality control halite deposition, rather than hydrologic forcing (Sirota et al., 2017, 2018).

Additionally, previously reported $\delta^{18}\text{O}$ and $\delta^{13}\text{C}$ from ~200 aragonite laminae recovered from MIS2 exposures of the Lisan Formation at Masada and Perazim Valley outerops were analyzedanalysed using wavelet analyses. Because the systematics of these isotopic compositions are distinctly different, these proxies bear different implication on environmental conditions in the

620 lake and its surroundings. More specifically, $\delta^{18}\text{O}$ is directly influenced by hydroclimatology, whereas $\delta^{13}\text{C}$ is primarily
 affected by biological activity (Kolodny et al., 2005). Nevertheless, it appears that because the extent of biological activity in
 Lake Lisan depended on freshwater inflow that also replenished its surface water with required nutrients (Begin et al., 2004),
 the two proxies share similar pacing and are broadly characterized by non-persistent ~~periodic~~ band of cyclicities of annual to
 decadal time scales that fail the cumulative area-wise significance test at the $\alpha=0.05$ level, although the coherence of this band
 625 between the signals is significant, and shows similar phase relationship (Fig. 9).

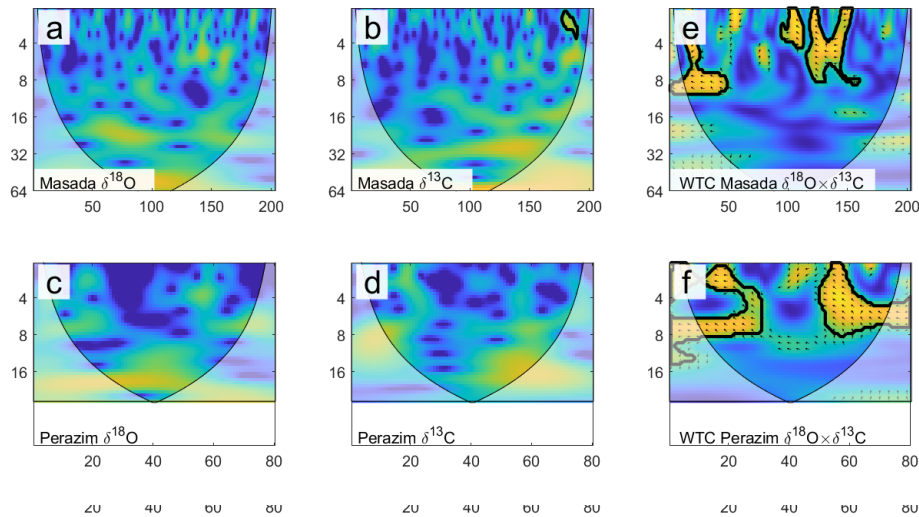


Figure 9 — Wavelet (a-d) and cross-wavelet (e-f) analyses of $\delta^{18}\text{O}$ and $\delta^{13}\text{C}$ in two segments of the Masada (30 ka) and Perazim (25 ka) exposures of the White Cliff Member (Lisan Formation) deposited during the last glacial over the lake's shelf. Areas with significance level above 0.95 ($\alpha=0.05$) are marked by a thick black line. Data is from (Kolodny et al., 2005).

– Wavelet (a-d) and cross-wavelet (e-f) analyses of $\delta^{18}\text{O}$ and $\delta^{13}\text{C}$ in two segments of the Masada (30 ka) and Perazim (25 ka) exposures of the White Cliff Member (Lisan Formation) deposited during the last glacial over the lake's shelf. Areas with significance level above 0.95 ($\alpha=0.05$) are marked by a thick black line. Data is from Kolodny et al. (2005).

The North Atlantic oscillation (NAO) and the Eastern Atlantic (EA) patterns were considered to affect interannual precipitation variability over the eastern Mediterranean (Feldstein and Dayan, 2008; Feliks et al., 2010; Krichak et al., 2002; Seager et al., 2019), primarily due to their reported effect on discrete precipitation-bearing synoptic patterns over the eastern Mediterranean (e.g., Black, 2012). Other studies, on the other hand, have suggested that unlike western Turkey, NAO shows only minimal direct impact on precipitation in the Levant, and that it might affect temperature instead (Enzel et al., 2003; Seager et al., 2020; Ziv et al., 2006). Although such relationships are hard to identify in geological records, a North Atlantic impact over the Dead Sea hydrology during the last glacial was identified by lake level reconstructions, where abrupt lake level drops took place during Heinrich events (Bartov et al., 2003). Additionally, a periodic component of a sub-decadal to decadal frequency bands (4-5, 7-8 and ~11 years) was also identified in laminated halite sequences deposited during the last interglacial and was attributed to NAO (Palchan et al., 2017). However, modern observations, may indicate that this pacing is manifested by temperature variations, which bear determine halite deposition, rather than hydrologic forcing (Sirota et al., 2017, 2018).

Century-long precipitation data from the Kfar Giladi and Jerusalem stations correlate well with pre-regulated modern Dead Sea levels, and are thus considered as recorders of to reflect mean hydrological conditions over the northern and central parts of the Dead Sea watershed in recent and past times (Enzel et al., 2003; Morin et al., 2019). Thus, available precipitation records in both stations were also compared to the winter (DJF) NAO and EA indices using wavelet and wavelet coherence in order

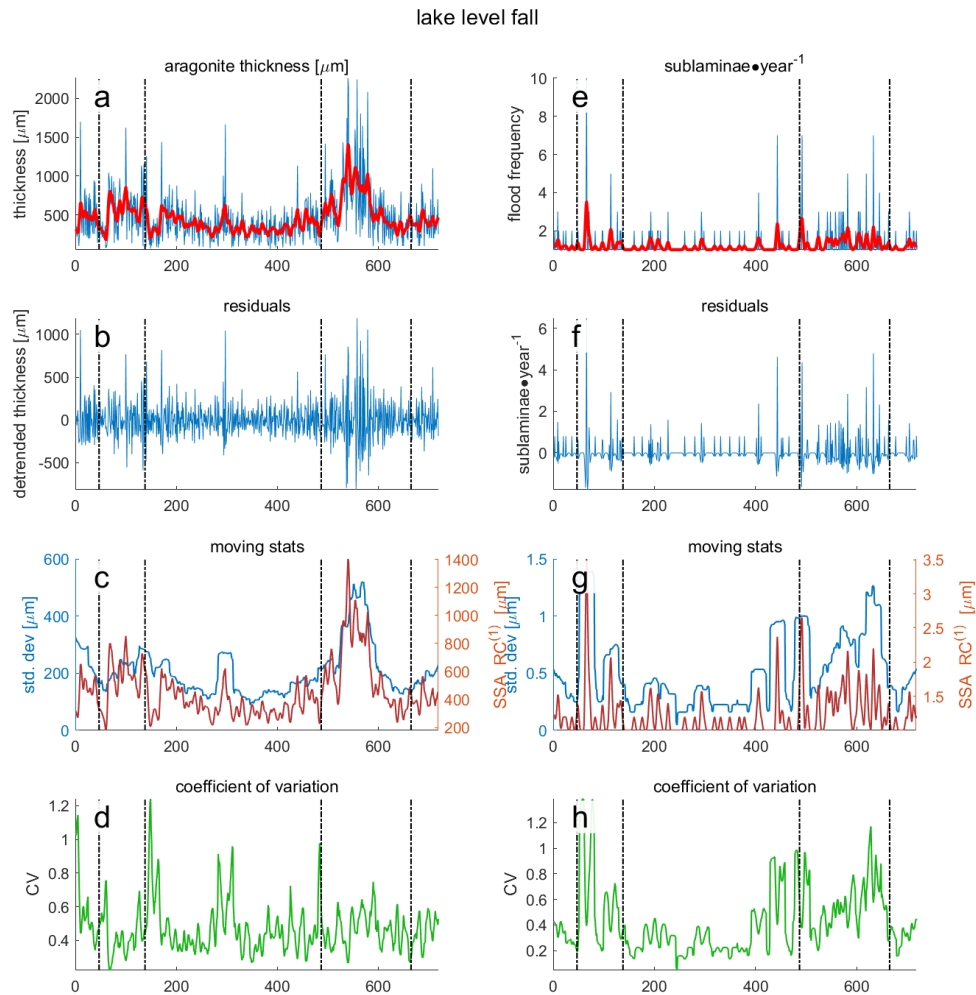
to detect common pacing and ~~periodic~~ periodic components (Figs. S15 and S16; NOAA, 2020). These relatively short records ~~are~~ do not exhibit significant ~~periodic~~ periodic components ~~in the series~~, and no significant coherence as well. However, although the available records do not exhibit significant ~~periodic~~ periodic behaviour (at $\alpha=0.05$), increased non-significant spectral power of short-term fluctuations are evident in the ICDP-DSDDP cores (Figs. 8, S6, S10-S13), in the isotopic composition of aragonite laminae (Fig. 9; Kolodny et al., 2005), ~~and in~~ modern precipitation records ~~and, as well as in the~~ winter indices of teleconnection patterns (Figs. S15 and S16). This ~~similarity that is not~~ statistically non-significant similarity, could either point at the lack of influence of NAO and EA on hydroclimate or at a weak and non-linear effect of these teleconnection patterns on precipitation in the eastern Mediterranean (Black, 2012). Alternatively, this can point at the inherent difficulties in ~~extracting~~ detecting such delicate relationships from sedimentary archives that ultimately record the interaction of complex hydrological and limnological processes involved in laminae formation and post depositional changes, such as the non-homogenous spread of fine-grained sediments over the lake floor and the effects of inflows from different catchments.

5.3 Clusters and regime transitions

The studied episodes demonstrate pronounced centennial-scale clustering of flooding events (Fig. 3). Similarly, other high-resolution palaeo-hydrological records (e.g., Witt et al., 2017) and modern observations (e.g., Metzger et al., 2020) have demonstrated non-uniform and non-~~Poisson~~ Poissonian flood frequencies. In addition, the clusters observed during lake-level fall are characterized by flood frequencies similar to those appearing in the background episodes during lake-level rise (Figs. S17 and S18). This suggests that the wetter episodes are characterized by increased mean precipitation and variability, as well as increased frequency of intense storms, which is in agreement with modern and more recent observations (Morin et al., 2019).

The comparison of aragonite laminae thickness of the two clusters identified in each of the studied intervals reveals opposing properties, which become evident when by comparing their $RC^{(1)}$ and dispersion, which is calculated as the running standard deviation of the residuals (after subtracting $RC^{(1)}$; Figs. 10 and 11). In each of the studied intervals, one cluster demonstrates increased mean and variance in both flood frequency and aragonite thickness, whereas the other cluster is characterized by increased mean flood frequency, but by maintains the mean and variance dispersion of aragonite thickness similar to that of background episodes (Figs. S17 and S18). In order to address these observations, a unified explanation that can account for this discrepancy is hereby suggested by considering the modern hydroclimatic regime and dominant synoptic circulation patterns.

Although modern records are relatively short, and the comparison of sparse hydrological measurements with the detailed framework of atmospheric circulation only permits cautious suggestions at this stage, the abovementioned observations can be explained using the modern synoptic framework by considering two distinct synoptic and hydroclimatic scenarios that govern flood generation and their clustering over the catchments that face the ICDP-DSDDP coring site. Most of the precipitation over the Dead Sea watershed is delivered by ~~extra-tropical cyclones~~ (Mediterranean lows) Lows during the winter months (e.g., Enzel et al., 2003; Saaroni et al., 2010; Ziv et al., 2006). When these cyclones are deep and have are characterized by a southern track, their ~~resulted~~ resulting precipitating clouds can pass have a pronounced impact on the Dead Sea watershed for longer periods and generate more rainfall, and therefore effectively deliver more precipitation to the watershed (Ziv et al., 2006; Saaroni et al., 2010). Thus, under these conditions they increase annual precipitation, while and at the same time increasing the chances of generating floods over the catchments that face the ICDP-DSDDP coring site (e.g., Armon et al., 2019; Belachsen et al., 2017; Goldreich, 2004). As suggested above, this scenario could account for the observed coupled increase in both mean and variance of flood frequency and aragonite laminae thickness, observed in one of the clusters in each of studied series (Fig. S17 and S18).



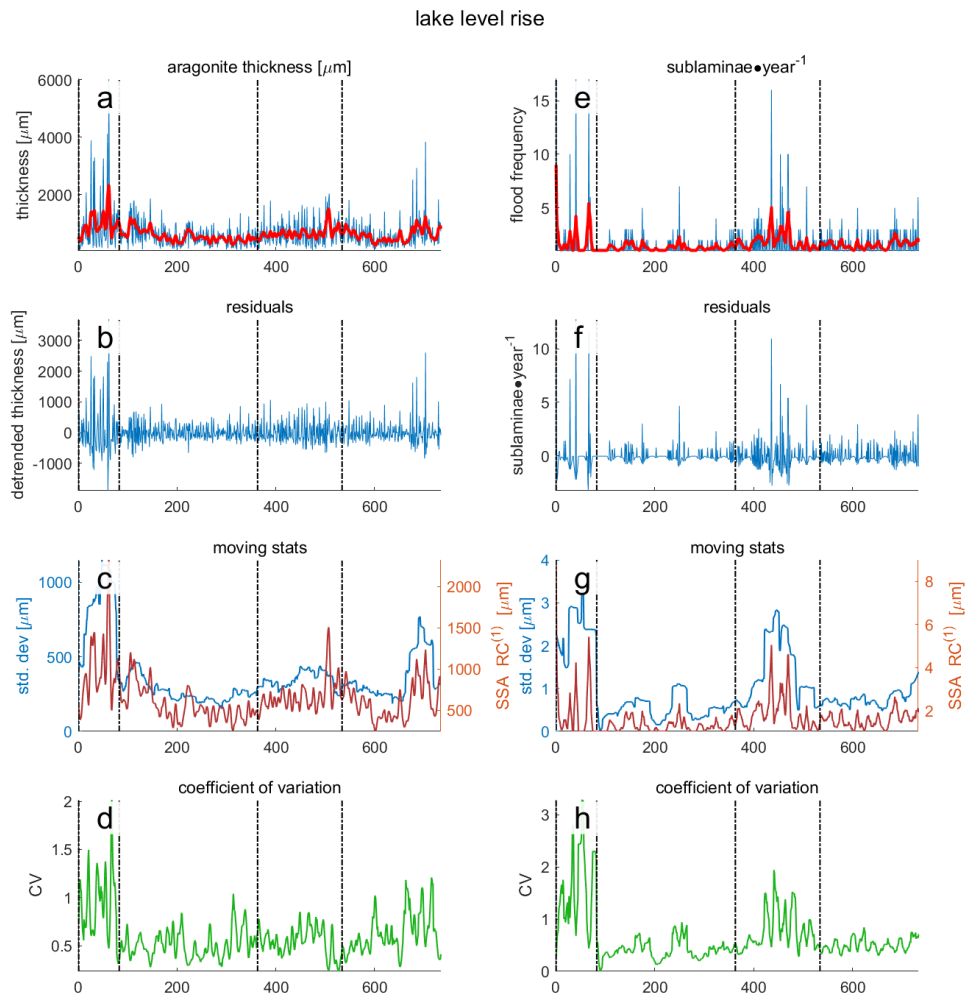
695 **Figure 10** –running statistical properties of aragonite laminae (a-d) and flood frequency (e-h) for the studied lake-level fall. (a,e) the
measured data (b,f), the residuals (after subtracting the $RC^{(1)}$ (c,g), $RC^{(1)}$ and running std. deviation (30 years window), and the
coefficient of variation calculated as $\frac{running\ std}{RC^{(1)}}$ (a,e) the measured data (b,f), the residuals (after subtracting the $RC^{(1)}$,
(e,g), $RC^{(1)}$ and running std. deviation (30 years window), and the coefficient of variation calculated as $\frac{std}{RC^{(1)}}$ (d,h).

700 The general understanding of precipitation patterns induced by different synoptic systems in the Dead Sea watershed depicts
a “de-coupling” of annual inflow into the lake, which depends on annual precipitation over the northern parts of the watershed,
and floods reaching the coring site. This is because the frequency and intensity of ~~(mainly eastern) Mediterranean Lows~~
determines annual precipitation over the watershed (Saaroni et al., 2010) and flood frequency in the relevant ephemeral streams
(Goldreich et al., 2004), whereas the contribution of the other synoptic systems to annual precipitation is, by far, is less
705 substantial (Armon et al., 2019; Marra et al., 2021). This is also evident by the low correlation ($r^2 = 0.086$) of major floods
(defined as flood peaks with return period >5 years) in the Negev Desert (Kahana et al., 2002) and precipitation in Jerusalem
(Fig. R1), which found to be is closely correlated with Dead Sea lake level, and hence with annual inflow into the lake (Enzel
et al., 2003). Thus, although this cannot be directly proven for the LGM, these modern observations are hereby considered
here as means to decipher the sedimentary record (e.g., Enzel et al., 2008; Goldsmith et al., 2017).

710

During the other cluster, on the other hand, the observed increased flood frequency is not coupled with increased mean and
variance of aragonite laminae thickness. Studies of modern floods and their synoptic settings indicate that floods over the
eastern Mediterranean are also generated by two other additional synoptic systems: the active Red Sea trough (ARST) and

715 disturbances to the subtropical jet stream (or Tropical Plumes). These synoptic conditions can generate significant floods over
 the small catchments surrounding the ICDP-DSDDP coring site, thus having the potential to deliver sediments, but owing to
 their spatiotemporal properties and frequency, they provide negligible contribution to total annual inflow into the lake (Armon
 et al., 2019). Under current conditions, ARSTs are more frequent than Tropical Plumes, and are characterized by high peak
 discharge and floods of relatively low volume floods—(e.g., Armon et al., 2018; Shentsis et al., 2012)—the. The second cluster
 may be therefore explained by increased frequency of ARSTs during decades of decreased mean annual precipitation. This
 720 scenario would result in increased flood frequency, recorded by more sub-laminae, without substantially increasing annual
 inflow, thus exhibiting aragonite thicknesses similar to background periods.



725 **Figure 11 – running statistical properties of aragonite laminae (a-d) and flood frequency (e-h) for the studied lake level rise.** ~~(a,e) the measured data (b,f), the residuals (after subtracting the $RC^{(+)}$) (c,g), $RC^{(+)}$ and running std. deviation (30 years window), and the coefficient of variation calculated as $\frac{std}{RC^{(+)}}$~~ (a,e) the measured data (b,f), the residuals (after subtracting the $RC^{(1)}$) (c,g), $RC^{(1)}$ and running std. deviation (30 years window), and the coefficient of variation calculated as $\frac{running\ std}{RC^{(1)}}$ (d,h).

6 Conclusions

The short-term hydroclimatic variability of opposing climatic trends in the Levant was studied in detail through several analyses of two annually-resolved varve sequences of the ICDP-DSDDP cores, representing opposing mean climates recorded by contrasting lake level trends. This unique sedimentary record complements the otherwise short and sparse modern climatic and hydrological records, and elucidates aspects and properties of regional hydroclimatology on centennial time scale. By the
 730 analyses of two sedimentary proxies that reflect annual inflow and flood frequency, and by their comparison with modern

climatic data and synoptic observations, new insights on hydroclimatic stationarity during late Pleistocene climate changes were revealed. These findings improve our understanding of short-term late Pleistocene hydroclimatic variability.

Key conclusions arise:

- 735 1. The ~~dispersion~~variance of both aragonite laminae thickness and flood frequency in the ICDP-DSDDP cores change with their mean, as observed in modern hydrologic ~~observations~~records. These findings strengthen the interpretation of these proxies as recorders of hydroclimatic phenomena in the Dead Sea watershed. During the “wetter” interval, which is characterized by lake-level rise, both the mean and the variance of these proxies are larger than during the studied episode of falling lake level.
- 740 2. No significant ~~periodic~~ycyclical components were identified in the studied records using singular spectrum, wavelet and recurrence analyses. However, it is suggested that this could stem from the interaction of climatic, hydrologic, and limnogeological processes that may have increased the noise/signal ratio of the studied proxies. ~~Thus~~Nevertheless, the integration of these methods suggest that some short-term oscillatory components could have affected annual precipitation and flood frequency during the late Pleistocene, but were not found to be significant in
- 745 the studied sedimentary sections.
- 750 3. Flood frequencies demonstrate ~~hydro-climatological~~hydroclimatic regime shifts operating at the centennial time scale. Floods are clustered into episodes ~~of~~that depict two distinct relationships between the mean and the dispersion of flood frequency and annual inflow. Namely, in each studied series one cluster is characterized by increased mean and variance of the two proxies, whereas the other cluster is characterized by increased mean and dispersion of flood frequency, ~~but~~which is not observed in annual precipitation. This implies that one of the clusters were generated by a distinct hydroclimatic regime, that was characterized by a different dominance of synoptic circulation patterns ~~that~~, which resulted in increased floods frequency at the decadal-scale, but without increasing annual precipitation. ~~More specifically~~Thus, it may suggest that clusters of increased flood frequencies could result either ~~result~~from ~~the~~ increased frequency of Mediterranean Lows or of Active Red Sea Troughs. Such regime shifts could also affect
- 755 modern and future conditions that would manifest as drastic hydroclimatic shifts at decadal to centennial scales.

Code availability

~~All code that was used for this research is available upon request from the corresponding author.~~

The code utilized for this research is available upon request from the corresponding author. Some of the analyses utilize available scripts and packages for wavelet analyses (Schulte, 2019, 2016; Grinsted et al., 2004; Torrence and Compo, 1998; 760 Schulte et al., 2018), SSA (e.g., <https://dept.atmos.ucla.edu/tcd/ssa-tutorial-matlab>), and recurrence plots and their analyses (Marwan, 2016; Marwan et al., 2007) using MATLAB.

Data availability

~~All the~~The data ~~that was~~used for this research is available ~~in the appendices or~~ upon request from the corresponding author.

Competing interests

765 The authors declare that they have no conflict of interest.

Acknowledgements

This study is a contribution to the PALEX project “Paleohydrology and Extreme Floods from the Dead Sea ICDP core”, funded by the DFG to A. Brauer, Y. Enzel, E. Morin, and Y. Erel (grant no. BR2208/13-1/-2). The authors acknowledge the support and contribution of laboratory staff and technicians in the GFZ, where preparation of thin-sections and photography were carried. We thank J. Mingham, N. Nowaczyk, B. Brademann, F. Ott, N. Dräger and M. Köppel for technical support and fruitful discussions. Y.B. is also grateful for a scholarship from the Advanced School of Environmental Studies, the Hebrew University of Jerusalem, ~~and~~ from the Rieger Foundation-Jewish National Fund program for environmental studies-, [and for the support of the Pfeiffer grant for postdoctoral fellows at the Institute of Earth Sciences at the Hebrew University of Jerusalem. We are grateful for the comments made by R. Donner, several anonymous reviewers, and the handling editor P. Francus during the review process, which altogether have improved the manuscript substantially.](#)

References

- Ahlborn, M., Armon, M., Ben Dor, Y., Neugebauer, I., Schwab, M. J., Tjallingii, R., Shoqeir, J. H., Morin, E., Enzel, Y., and Brauer, A.: Increased frequency of torrential rainstorms during a regional late Holocene eastern Mediterranean drought, *Quaternary Research*, 89, 425-431, 10.1017/qua.2018.9, 2018.
- Allen, K., Hope, P., Lam, D., Brown, J., and Wasson, R.: Improving Australia’s flood record for planning purposes—can we do better?, *Australasian Journal of Water Resources*, 24, 36-45, 2020.
- Alpert, P., Ben-Gai, T., Baharad, A., Benjamini, Y., Yekutieli, D., Colacino, M., Diodato, L., Ramis, C., Homar, V., Romero, R., Michaelides, S., and Manes, A.: The paradoxical increase of Mediterranean extreme daily rainfall in spite of decrease in total values, *Geophysical Research Letters*, 29, 31-31-31-34, 10.1029/2001GL013554, 2002.
- Amit, R., Simhai, O., Ayalon, A., Enzel, Y., Matmon, A., Crouvi, O., Porat, N., and McDonald, E.: Transition from arid to hyper-arid environment in the southern Levant deserts as recorded by early Pleistocene cummulic Aridisols, *Quaternary Science Reviews*, 30, 312-323, 2011.
- Ansari, A. R. and Bradley, R. A.: Rank-sum tests for dispersions, *The Annals of Mathematical Statistics*, 31, 1174-1189, 1960.
- Armon, M., morin, E., and Enzel, Y.: Overview of modern atmospheric patterns controlling rainfall and floods into the Dead Sea: Implications for the lake’s sedimentology and paleohydrology, *Quaternary Science Reviews*, 216, 58-73, 2019.
- Armon, M., Dente, E., Smith, J. A., Enzel, Y., and Morin, E.: Synoptic-Scale Control over Modern Rainfall and Flood Patterns in the Levant Drylands with Implications for Past Climates, *Journal of Hydrometeorology*, 19, 1077-1096, 10.1175/jhm-d-18-0013.1, 2018.
- Armon, M., Marra, F., Enzel, Y., Rostkier-Edelstein, D., and Morin, E.: Radar-based characterisation of heavy precipitation in the eastern Mediterranean and its representation in a convection-permitting model, *Hydrology and Earth System Sciences*, 24, 1227-1249, 2020.
- Avni, S., Joseph-Hai, N., Haviv, I., Matmon, A., Benedetti, L., and Team, A.: Patterns and rates of 103–105 yr denudation in carbonate terrains under subhumid to subalpine climatic gradient, Mount Hermon, Israel, *Bulletin*, 131, 899-912, 2018.
- Baker, V. R.: Paleoflood hydrology: Origin, progress, prospects, *Geomorphology*, 101, 1-13, 2008.
- Bar-Matthews, M., Ayalon, A., Kaufman, A., and Wasserburg, G. J.: The Eastern Mediterranean paleoclimate as a reflection of regional events: Soreq cave, Israel, *Earth Planet. Sci. Lett.*, 166, 85-95, 1999.
- Bar-Matthews, M., Ayalon, A., Gilmour, M., Matthews, A., and Hawkesworth, C. J.: Sea–land oxygen isotopic relationships from planktonic foraminifera and speleothems in the Eastern Mediterranean region and their implication for paleorainfall during interglacial intervals, *Geochim. Cosmochim. Acta*, 67, 3181-3199, 2003.
- Bartov, Y., Enzel, Y., Porat, N., and Stein, M.: Evolution of the Late Pleistocene–Holocene Dead Sea Basin from sequence stratigraphy of fan deltas and lake-level reconstruction, *Journal of Sedimentary Research*, 77, 680-692, 2007.

- Bartov, Y., Goldstein, S. L., Stein, M., and Enzel, Y.: Catastrophic arid episodes in the Eastern Mediterranean linked with the North Atlantic Heinrich events, *Geology*, 31, 439-442, 2003.
- 825 Bartov, Y., Stein, M., Enzel, Y., Agnon, A., and Reches, Z.: Lake levels and sequence stratigraphy of Lake Lisan, the Late Pleistocene precursor of the Dead Sea, *Quaternary Research*, 57, 9-21, 2002.
- Begin, Z., Ehrlich, A., and Nathan, Y.: Lake Lisan: the Pleistocene precursor of the Dead Sea, Ministry of Commerce and Industry, Geological Survey of Israel, Jerusalem, 45, 1974.
- 830 Begin, Z. B., Nathan, Y., and Ehrlich, A.: Stratigraphy and facies distribution in the Lisan Formation—new evidence from the area south of the Dead Sea, Israel, *Israel Journal of Earth Sciences*, 29, 182-189, 1980.
- Begin, Z. B., Stein, M., Katz, A., Machlus, M., Rosenfeld, A., Buchbinder, B., and Bartov, Y.: Southward migration of rain tracks during the last glacial, revealed by salinity gradient in Lake Lisan (Dead Sea rift), *Quaternary Science Reviews*, 23, 1627-1636, 10.1016/j.quascirev.2004.01.002, 2004.
- 835 Belachsen, I., Marra, F., Peleg, N., and Morin, E.: Convective rainfall in dry climate: relations with synoptic systems and flash-flood generation in the Dead Sea region, *Hydrol. Earth Syst. Sci. Discuss*, 2017.
- 840 Belmaker, R., ~~Taha, N., and Bookman, R.: Evidence for aragonite deposition in flood plumes of the Dead Sea, Goldschmidt Abstract 196,~~
- ~~Belmaker, R.,~~ Lazar, B., Stein, M., Taha, N., and Bookman, R.: Constraints on aragonite precipitation in the Dead Sea from geochemical measurements of flood plumes, *Quaternary Science Reviews*, 221, 105876, 2019.
- 845 Ben David-Novak, H., Morin, E., and Enzel, Y.: Modern extreme storms and the rainfall thresholds for initiating debris flows on the hyperarid western escarpment of the Dead Sea, Israel, *Geological Society of America Bulletin*, 116, 718-728, 2004.
- 850 Ben Dor, Y., Flax, T., Levitan, I., Enzel, Y., Brauer, A., and Erel, Y.: The paleohydrological implications of aragonite precipitation under contrasting climates in the endorheic Dead Sea and its precursors revealed by experimental investigations, *Chemical Geology*, 576, 10.1016/j.chemgeo.2021.120261, 2021.
- 855 Ben Dor, Y., Neugebauer, I., Enzel, Y., Schwab, M. J., Tjallingii, R., Erel, Y., and Brauer, A.: Varves of the Dead Sea sedimentary record, *Quaternary Science Reviews*, 215, 173-184, 2019.
- Ben Dor, Y., Neugebauer, I., Enzel, Y., Schwab, M. J., Tjallingii, R., Erel, Y., and Brauer, A.: Reply to comment on Ben Dor Y. et al. "Varves of the Dead Sea sedimentary record." *Quaternary Science Reviews* 215 (2019): 173–184, *Quaternary Science Reviews*, 231, 10.1016/j.quascirev.2019.106063, 2020.
- 860 Ben Dor, Y., Armon, M., Ahlborn, M., Morin, E., Erel, Y., Brauer, A., Schwab, M. J., Tjallingii, R., and Enzel, Y.: Changing flood frequencies under opposing late Pleistocene eastern Mediterranean climates, *Sci Rep*, 8, 8445, 10.1038/s41598-018-25969-6, 2018.
- 865 Black, E.: The influence of the North Atlantic Oscillation and European circulation regimes on the daily to interannual variability of winter precipitation in Israel, *International Journal of Climatology*, 32, 1654-1664, 2012.
- Blackman, R. B. and Tukey, J. W.: The measurement of power spectra, 1958.
- 870 Bookman, R., Bartov, Y., Enzel, Y., and Stein, M.: Quaternary lake levels in the Dead Sea basin: two centuries of research, *Geological Society of America Special Papers*, 401, 155-170, 2006.
- Brauer, A., Endres, C., and Negendank, J. F.: Lateglacial calendar year chronology based on annually laminated sediments from Lake Meerfelder Maar, Germany, *Quaternary International*, 61, 17-25, 1999.
- 875 Brauer, A., Mangili, C., Moscariello, A., and Witt, A.: Palaeoclimatic implications from micro-facies data of a 5900 varve time series from the Piànico interglacial sediment record, southern Alps, *Palaeogeography, Palaeoclimatology, Palaeoecology*, 259, 121-135, 2008.
- 880 Broomhead, D. S. and King, G. P.: Nonlinear phenomena and chaos, *On the Qualitative Analysis of Experimental Dynamical Systems*, Malvern science series, Bristol, UK, 113-144, 1986.
- Campins, J., Genovés, A., Picornell, M., and Jansà, A.: Climatology of Mediterranean cyclones using the ERA-40 dataset, *International Journal of Climatology*, 31, 1596-1614, 2011.
- 885

- Coianiz, L., Ben-Avraham, Z., Stein, M., and Lazar, M.: Spatial and temporal reconstruction of the late Quaternary Dead Sea sedimentary facies from geophysical properties, *Journal of Applied Geophysics*, 160, 15-27, 2019.
- 890 Crouvi, O., Amit, R., Ben Israel, M., and Enzel, Y.: Loess in the Negev desert: sources, loessial soils, palaeosols, and palaeoclimatic implications, in: *Quaternary of the Levant: Environments, Climate Change, and Humans*. Cambridge University Press, Cambridge, edited by: Enzel, Y., and Bar-Yosef, O., 471-482, 2017.
- 895 Dayan, U. and Morin, E.: Flash flood-producing rainstorms over the Dead Sea: A review, *Geological Society of America Special Papers*, 401, 53-62, 2006.
- 900 Dean, J. R., Eastwood, W. J., Roberts, N., Jones, M. D., Yiğitbaşıoğlu, H., Allcock, S. L., Woodbridge, J., Metcalfe, S. E., and Leng, M. J.: Tracking the hydro-climatic signal from lake to sediment: A field study from central Turkey, *Journal of Hydrology*, 529, 608-621, 2015.
- 905 Donges, J. F., Donner, R. V., Trauth, M. H., Marwan, N., Schellnhuber, H.-J., and Kurths, J.: Nonlinear detection of paleoclimate-variability transitions possibly related to human evolution, *Proceedings of the National Academy of Sciences*, 108, 20422-20427, 2011.
- 910 Drori, R., Ziv, B., Saaroni, H., Etkin, A., and Sheffer, E.: Recent changes in the rain regime over the Mediterranean climate region of Israel, *Climatic Change*, 167, 15, 10.1007/s10584-021-03161-6, 2021.
- 915 Enzel, Y., Amit, R., Dayan, U., Crouvi, O., Kahana, R., Ziv, B., and Sharon, D.: The climatic and physiographic controls of the eastern Mediterranean over the late Pleistocene climates in the southern Levant and its neighboring deserts, *Global and Planetary Change*, 60, 165-192, 2008.
- 920 Enzel, Y., Bookman, R., Sharon, D., Gvirtzman, H., Dayan, U., Ziv, B., and Stein, M.: Late Holocene climates of the Near East deduced from Dead Sea level variations and modern regional winter rainfall, *Quaternary Research*, 60, 263-273, 2003.
- 925 Enzel, Y., Amit, R., Grodek, T., Ayalon, A., Lekach, J., Porat, N., Bierman, P., Blum, J. D., and Erel, Y.: Late Quaternary weathering, erosion, and deposition in Nahal Yael, Israel: An “impact of climatic change on an arid watershed”?, *Bulletin*, 124, 705-722, 2012.
- 930 Feldstein, S. B. and Dayan, U.: Circumglobal teleconnections and wave packets associated with Israeli winter precipitation, *Quarterly Journal of the Royal Meteorological Society: A journal of the atmospheric sciences, applied meteorology and physical oceanography*, 134, 455-467, 2008.
- 935 Feliks, Y., Ghil, M., and Robertson, A. W.: Oscillatory climate modes in the Eastern Mediterranean and their synchronization with the North Atlantic Oscillation, *Journal of Climate*, 23, 4060-4079, 2010.
- 940 Flocas, H. A., Simmonds, I., Kouroutzoglou, J., Keay, K., Hatzaki, M., Bricolas, V., and Asimakopoulos, D.: On cyclonic tracks over the eastern Mediterranean, *Journal of Climate*, 23, 5243-5257, 2010.
- 945 Ganor, E. and Foner, H.: The mineralogical and chemical properties and the behaviour of aeolian Saharan dust over Israel, in: *The impact of desert dust across the Mediterranean*, Springer, 163-172, 1996.
- 950 Garber, R. A., Levy, Y., and Friedman, G. M.: The sedimentology of the Dead Sea, Carbonates and Evaporites, 2, 43-57, 1987.
- 955 Garfunkel, Z.: Internal structure of the Dead Sea leaky transform (rift) in relation to plate kinematics, *Tectonophysics*, 80, 81-108, 1981.
- 960 Garfunkel, Z. and Ben-Avraham, Z.: The structure of the Dead Sea basin, *Tectonophysics*, 266, 155-176, 1996.
- 965 Ghil, M., Allen, M., Dettinger, M., Ide, K., Kondrashov, D., Mann, M., Robertson, A. W., Saunders, A., Tian, Y., and Varadi, F.: Advanced spectral methods for climatic time series, *Reviews of geophysics*, 40, 2002.
- 970 ~~Golan, R., Lazar, B., Wurgaft, E., Lensky, N., Ganor, J., and Gavrieli, I.: Continuous CO₂ escape from the hypersaline Dead Sea caused by aragonite precipitation, *Geochim. Cosmochim. Acta*, 207, 43-56, 10.1016/j.gea.2017.02.031, 2017.~~
- 975 Goldreich, Y.: Spatial Distribution of Mid-season Rainfall Date in Israel - a Review, *Horizons in Geography*, 177-182, 2004.

- 950 Goldreich, Y.: The climate of Israel: observation, research and application, Springer Science & Business Media 2012.
- Goldreich, Y., Mozes, H., and Rosenfeld, D.: Radar analysis of cloud systems and their rainfall yield in Israel, *Isr. J. Earth Sci.*, 53, 63-76, 2004.
- 955 Goldsmith, Y., Polissar, P., Ayalon, A., Bar-Matthews, M., and Broecker, W.: The modern and Last Glacial Maximum hydrological cycles of the Eastern Mediterranean and the Levant from a water isotope perspective, *Earth Planet. Sci. Lett.*, 457, 302-312, 2017.
- 960 Greenbaum, N., Schwartz, U., and Bergman, N.: Extreme floods and short-term hydroclimatological fluctuations in the hyper-arid Dead Sea region, Israel, *Global and Planetary Change*, 70, 125-137, 2010.
- Greenbaum, N., Ben-Zvi, A., Haviv, I., and Enzel, Y.: The hydrology and paleohydrology of the Dead Sea tributaries, *Geological Society of America Special Papers*, 401, 63-93, 2006.
- 965 Grinsted, A., Moore, J. C., and Jevrejeva, S.: Application of the cross wavelet transform and wavelet coherence to geophysical time series, *Nonlinear processes in geophysics*, 11, 561-566, <https://doi.org/10.5194/npg-11-561-2004>, 2004.
- 970 Haase-Schramm, A., Goldstein, S. L., and Stein, M.: U-Th dating of Lake Lisan (late Pleistocene dead sea) aragonite and implications for glacial east Mediterranean climate change, *Geochim. Cosmochim. Acta*, 68, 985-1005, <http://dx.doi.org/10.1016/j.gca.2003.07.016>, 2004.
- Heim, C., Nowaczyk, N. R., Negendank, J. F., Leroy, S. A., and Ben-Avraham, Z.: Near East desertification: evidence from the Dead Sea, *Naturwissenschaften*, 84, 398-401, 1997.
- 975 Held, I. M. and Soden, B. J.: Robust responses of the hydrological cycle to global warming, *Journal of Climate*, 19, 5686-5699, 2006.
- 980 Hochman, A., Saaroni, H., Abramovich, F., and Alpert, P.: Artificial Detection of Lower-Frequency Periodicity in Climatic Studies by Wavelet Analysis Demonstrated on Synthetic Time Series, *Journal of Applied Meteorology and Climatology*, 58, 2077-2086, 2019.
- 985 IPCC, Zhai, V. P., Pirani, A. S., Connors, L., Péan, C., Berger, S., Caud, N., Chen, Y., Goldfarb, L., Gomis, M. I., Huang, M., Leitzell, K., Lonnoy, J. B. E., Matthews, R., Maycock, T. K., Waterfield, T., Yelekçi, O., Yu, R., and Zhou, B. (Eds.): *Climate Change 2021: The Physical Science Basis*, Cambridge University Press. In Press 2021.
- Kagan, E., Stein, M., and Marco, S.: Integrated Paleoseismic Chronology of the Last Glacial Lake Lisan: From Lake Margin Seismites to Deep-Lake Mass Transport Deposits, *Journal of Geophysical Research: Solid Earth*, 10.1002/2017JB014117, 2018.
- 990 Kahana, R., Ziv, B., Enzel, Y., and Dayan, U.: Synoptic climatology of major floods in the Negev Desert, Israel, *International Journal of Climatology*, 22, 867-882, 2002.
- 995 Kalderon-Asael, B., Erel, Y., Sandler, A., and Dayan, U.: Mineralogical and chemical characterization of suspended atmospheric particles over the east Mediterranean based on synoptic-scale circulation patterns, *Atmospheric Environment*, 43, 3963-3970, 2009.
- 1000 Katz, A., Kolodny, Y., and Nissenbaum, A.: The geochemical evolution of the Pleistocene Lake Lisan-Dead Sea system, *Geochim. Cosmochim. Acta*, 41, 1609-1626, 10.1016/0016-7037(77)90172-7, 1977.
- Kaufman, A.: U-Series dating of Dead Sea Basin carbonates, *Geochim. Cosmochim. Acta*, 35, 1269-1281, [http://dx.doi.org/10.1016/0016-7037\(71\)90115-3](http://dx.doi.org/10.1016/0016-7037(71)90115-3), 1971.
- 1005 Keinan, J., Bar-Matthews, M., Ayalon, A., Zilberman, T., Agnon, A., and Frumkin, A.: Paleoclimatology of the Levant from Zalmon Cave speleothems, the northern Jordan Valley, Israel, *Quaternary Science Reviews*, 220, 142-153, 2019.
- Kelley, C., Ting, M., Seager, R., and Kushnir, Y.: Mediterranean precipitation climatology, seasonal cycle, and trend as simulated by CMIP5, *Geophysical Research Letters*, 39, 2012.
- 1010 Kennel, M. B., Brown, R., and Abarbanel, H. D.: Determining embedding dimension for phase-space reconstruction using a geometrical construction, *Physical review A*, 45, 3403, 1992.

- 1015 Kitagawa, H., Stein, M., Goldstein, S. L., Nakamura, T., and Lazar, B.: Radiocarbon chronology of the DSDDP core at the deepest floor of the Dead Sea, *Radiocarbon*, 59, 383-394, 10.1017/RDC.2016.120, 2017.
- Kolodny, Y., Stein, M., and Machlus, M.: Sea-rain-lake relation in the Last Glacial East Mediterranean revealed by $\delta^{18}\text{O}$ - $\delta^{13}\text{C}$ in Lake Lisan aragonites, *Geochim. Cosmochim. Acta*, 69, 4045-4060, 10.1016/j.gca.2004.11.022, 2005.
- 1020 Kondrashov, D. and Ghil, M.: Spatio-temporal filling of missing points in geophysical data sets, *Nonlinear Processes in Geophysics*, 13, 151-159, 2006.
- Kottek, M., Grieser, J., Beck, C., Rudolf, B., and Rubel, F.: World map of the Köppen-Geiger climate classification updated, *Meteorologische Zeitschrift*, 15, 259-263, 2006.
- 1025 Krichak, S., Kishcha, P., and Alpert, P.: Decadal trends of main Eurasian oscillations and the Eastern Mediterranean precipitation, *Theoretical and Applied Climatology*, 72, 209-220, 2002.
- Kushnir, Y., Dayan, U., Ziv, B., Morin, E., and Enzel, Y.: Climate of the Levant, in: *Quaternary of the Levant*, edited by: Enzel, Y., and Bar-Yosef, O., Cambridge University Press, Cambridge, 31-44, 10.1017/9781316106754.004, 2017.
- 1030 Lau, K. and Weng, H.: Climate signal detection using wavelet transform: How to make a time series sing, *Bulletin of the American Meteorological Society*, 76, 2391-2402, 1995.
- 1035 Le Mouél, J. L., Lopes, F., and Courtillot, V.: A Solar Signature in Many Climate Indices, *Journal of Geophysical Research: Atmospheres*, 2019.
- Levy, Y., Burg, A., Yechieli, Y., and Gvirtzman, H.: Displacement of springs and changes in groundwater flow regime due to the extreme drop in adjacent lake levels: The Dead Sea rift, *Journal of Hydrology*, 587, 10.1016/j.jhydrol.2020.124928, 2020.
- 1040 Lisiecki, L. E. and Raymo, M. E.: A Pliocene-Pleistocene stack of 57 globally distributed benthic $\delta^{18}\text{O}$ records, *Paleoceanography*, 20, 2005.
- 1045 Luck, M., Landis, M., and Gassert, F.: Aqueduct water stress projections: decadal projections of water supply and demand using CMIP5 GCMs, Technical Note. Washington, DC: World Resources Institute. Available online at: <http://www.wri.org/publication/aqueduct-waterstress-projections>, 2015.
- Luo, T., Young, R., and Reig, P.: Aqueduct Projected Water Stress Country Rankings, Technical Note, 2015.
- 1050 Machlus, M., Enzel, Y., Goldstein, S. L., Marco, S., and Stein, M.: Reconstructing low levels of Lake Lisan by correlating fan-delta and lacustrine deposits, *Quaternary International*, 73, 137-144, 2000.
- 1055 Mann, H. B. and Whitney, D. R.: On a test of whether one of two random variables is stochastically larger than the other, *The annals of mathematical statistics*, 50-60, 1947.
- Marco, S., Stein, M., Agnon, A., and Ron, H.: Long-term earthquake clustering: A 50,000-year paleoseismic record in the Dead Sea Graben, *Journal of Geophysical Research: Solid Earth*, 101, 6179-6191, 1996.
- 1060 Marra, F., Armon, M., Adam, O., Zoccatelli, D., Gazal, O., Garfinkel, C. I., Rostkier-Edelstein, D., Dayan, U., Enzel, Y., and Morin, E.: Toward Narrowing Uncertainty in Future Projections of Local Extreme Precipitation, *Geophysical Research Letters*, 48, e2020GL091823, 2021.
- 1065 Marwan, N.: How to avoid potential pitfalls in recurrence plot based data analysis, *International Journal of Bifurcation and Chaos*, 21, 1003-1017, 2011.
- Marwan, N.: [Cross Recurrence Plot Toolbox for Matlab \[code\]. 2016.](#)
- 1070 [Marwan, N.](#) and Kurths, J.: Cross recurrence plots and their applications, *Mathematical physics research at the cutting edge*, 101-139, 2004.
- Marwan, N., Romano, M. C., Thiel, M., and Kurths, J.: Recurrence plots for the analysis of complex systems, *Physics reports*, 438, 237-329, 2007.
- 1075 Marwan, N., Trauth, M. H., Vuille, M., and Kurths, J.: Comparing modern and Pleistocene ENSO-like influences in NW Argentina using nonlinear time series analysis methods, *Climate Dynamics*, 21, 317-326, 2003.

- Metzger, A., Marra, F., Smith, J. A., and Morin, E.: Flood frequency estimation and uncertainty in arid/semi-arid regions, *Journal of Hydrology*, 590, 125254, 2020.
- 1080 Migowski, C., Stein, M., Prasad, S., Negendank, J. F., and Agnon, A.: Holocene climate variability and cultural evolution in the Near East from the Dead Sea sedimentary record, *Quaternary Research*, 66, 421-431, 2006.
- Morin, E.: To know what we cannot know: Global mapping of minimal detectable absolute trends in annual precipitation, *Water Resources Research*, 47, 2011.
- 1085 Morin, E., Ryb, T., Gavrieli, I., and Enzel, Y.: Mean, variance, and trends of Levant precipitation over the past 4500 years from reconstructed Dead Sea levels and stochastic modeling, *Quaternary Research*, 91, 751-767, 2019.
- Neev, D.: Recent precipitation of calcium salts in the Dead Sea, *Bull. Res. Council Israel, Sect. G*, 11, 153-154, 1963.
- 1090 Neev, D. and Emery, K. O.: The Dead Sea: depositional processes and environments of evaporites, Ministry of Commerce and Industry, Geological Survey of Israel, Jerusalem, 1967.
- Nehorai, R., Lensky, I., Hochman, L., Gertman, I., Brenner, S., Muskin, A., and Lensky, N.: Satellite observations of turbidity in the Dead Sea, *Journal of Geophysical Research: Oceans*, 118, 3146-3160, 2013.
- 1095 Neugebauer, I., Brauer, A., Schwab, M. J., Dulski, P., Frank, U., Hadzhiivanova, E., Kitagawa, H., Litt, T., Schiebel, V., and Taha, N.: Evidences for centennial dry periods at~ 3300 and~ 2800 cal. yr BP from micro-facies analyses of the Dead Sea sediments, *The Holocene*, 0959683615584208, 2015.
- 1100 Neugebauer, I., Brauer, A., Schwab, M. J., Waldmann, N. D., Enzel, Y., Kitagawa, H., Torfstein, A., Frank, U., Dulski, P., and Agnon, A.: Lithology of the long sediment record recovered by the ICDP Dead Sea Deep Drilling Project (DSDDP), *Quaternary Science Reviews*, 102, 149-165, 2014.
- 1105 Nissenbaum, A., Baedeker, M. J., and Kaplan, I. R.: Organic geochemistry of Dead Sea sediments, *Geochim. Cosmochim. Acta*, 36, 709-727, 1972.
- NOAA Climate Prediction Center, teleconnection patterns, [dataset],
 2020. <https://www.cpc.ncep.noaa.gov/data/teledoc/telecontents.shtml>
- 1110 Palchan, D., Neugebauer, I., Amitai, Y., Waldmann, N. D., Schwab, M. J., Dulski, P., Brauer, A., Stein, M., Erel, Y., and Enzel, Y.: North Atlantic controlled depositional cycles in MIS 5e layered sediments from the deep Dead Sea basin, *Quaternary Research*, 87, 168-179, 2017.
- 1115 Peleg, N., Bartov, M., and Morin, E.: CMIP5-predicted climate shifts over the East Mediterranean: implications for the transition region between Mediterranean and semi-arid climates, *International journal of climatology*, 35, 2144-2153, 2015.
- Prasad, S., Negendank, J., and Stein, M.: Varve counting reveals high resolution radiocarbon reservoir age variations in palaeolake Lisan, *Journal of Quaternary Science: Published for the Quaternary Research Association*, 24, 690-696, 2009.
- 1120 Prasad, S., Vos, H., Negendank, J., Waldmann, N., Goldstein, S. L., and Stein, M.: Evidence from Lake Lisan of solar influence on decadal-to centennial-scale climate variability during marine oxygen isotope stage 2, *Geology*, 32, 581-584, 2004.
- Redmond, K. T., Enzel, Y., House, P. K., and Biondi, F.: Climate variability and flood frequency at decadal to millennial time scales, *Ancient floods, modern hazards: principles and applications of paleoflood hydrology*, 5, 21-45, 2002.
- 1125 Roeser, P., Dräger, N., Brykała, D., Ott, F., Pinkerneil, S., Gierszewski, P., Lindemann, C., Plessen, B., Brademann, B., Kaszubski, M., Fojutowski, M., Schwab, M. J., Słowiński, M., Błaszkiwicz, M., and Brauer, A.: Advances in understanding calcite varve formation: new insights from a dual lake monitoring approach in the southern Baltic lowlands, *Boreas*, 10.1111/bor.12506, 2021.
- Rohling, E. J.: Quantitative assessment of glacial fluctuations in the level of Lake Lisan, Dead Sea rift, *Quaternary Science Reviews*, 70, 63-72, 10.1016/j.quascirev.2013.03.013, 2013.
- 1135 Romano, M. C., Thiel, M., Kurths, J., and von Bloh, W.: Multivariate recurrence plots, *Physics letters A*, 330, 214-223, 2004.
- Ryb, U., Matmon, A., Erel, Y., Haviv, I., Benedetti, L., and Hidy, A.: Styles and rates of long-term denudation in carbonate terrains under a Mediterranean to hyper-arid climatic gradient, *Earth Planet. Sci. Lett.*, 406, 142-152, 2014.
- 1140

- Saaroni, H., Halfon, N., Ziv, B., Alpert, P., and Kutiel, H.: Links between the rainfall regime in Israel and location and intensity of Cyprus lows, *International Journal of Climatology*, 30, 1014-1025, 2010.
- 1145 Safriel, U., Adeel, Z., Niemeijer, D., Puigdefabregas, J., White, R., Lal, R., Winslow, M., Ziedler, J., Prince, S., and Archer, E.: Dryland systems, in: *Ecosystems and Human Well-being: Current State and Trends.: Findings of the Condition and Trends Working Group*, Island Press, 623-662, 2005.
- 1150 Schinkel, S., Dimigen, O., and Marwan, N.: Selection of recurrence threshold for signal detection, *The european physical journal special topics*, 164, 45-53, 2008.
- Schulte, J. A.: Cumulative areawise testing in wavelet analysis and its application to geophysical time series, *Nonlinear Processes in Geophysics*, 23, 45-57, 2016.
- 1155 Schulte, J. A.: Statistical hypothesis testing in wavelet analysis: theoretical developments and applications to Indian rainfall, *Nonlinear Processes in Geophysics*, 26, 91-108, 2019.
- Schulte, J. A., Georgas, N., Saba, V., and Howell, P.: North Pacific influences on Long Island sound temperature variability, *Journal of Climate*, 31, 2745-2769, 2018.
- 1160 Seager, R., Osborn, T. J., Kushnir, Y., Simpson, I. R., Nakamura, J., and Liu, H.: Climate variability and change of Mediterranean-type climates, *Journal of Climate*, 32, 2887-2915, 2019.
- 1165 Seager, R., Liu, H., Kushnir, Y., Osborn, T. J., Simpson, I. R., Kelley, C. R., and Nakamura, J.: Mechanisms of Winter Precipitation Variability in the European–Mediterranean Region Associated with the North Atlantic Oscillation, *Journal of Climate*, 33, 7179-7196, 2020.
- Serinaldi, F., Kilsby, C. G., and Lombardo, F.: Untenable nonstationarity: An assessment of the fitness for purpose of trend tests in hydrology, *Advances in Water Resources*, 111, 132-155, 2018.
- 1170 Israel Meteorological Service, Climatic data in Israel (1995-2009), [dataset], 2021. <https://ims.gov.il/he/ClimateAtlas>
- Sharon, D.: The spottiness of rainfall in a desert area, *Journal of Hydrology*, 17, 161-175, 1972.
- 1175 Sharon, D. and Kutiel, H.: The distribution of rainfall intensity in Israel, its regional and seasonal variations and its climatological evaluation, *Journal of Climatology*, 6, 277-291, 1986.
- Shentsis, I., Laronne, J. B., and Alpert, P.: Red Sea Trough flood events in the Negev, Israel (1964–2007), *Hydrological sciences journal*, 57, 42-51, 2012.
- 1180 Shohami, D., Dayan, U., and Morin, E.: Warming and drying of the eastern Mediterranean: Additional evidence from trend analysis, *Journal of Geophysical Research: Atmospheres*, 116, 2011.
- 1185 Siebert, C., Rodiger, T., Mallast, U., Grabe, A., Guttman, J., Laronne, J. B., Storz-Peretz, Y., Greenman, A., Salameh, E., Al-Raggad, M., Vachtman, D., Zvi, A. B., Ionescu, D., Brenner, A., Merz, R., and Geyer, S.: Challenges to estimate surface- and groundwater flow in arid regions: the Dead Sea catchment, *Sci Total Environ*, 485-486, 828-841, 10.1016/j.scitotenv.2014.04.010, 2014.
- 1190 Sirota, I., Enzel, Y., and Lensky, N. G.: Temperature seasonality control on modern halite layers in the Dead Sea: In situ observations, *Geological Society of America Bulletin*, B31661. 31661, 2017.
- Sirota, I., Enzel, Y., and Lensky, N. G.: Halite focusing and amplification of salt layer thickness: From the Dead Sea to deep hypersaline basins, *Geology*, 2018.
- 1195 Stein, M., Starinsky, A., Katz, A., Goldstein, S. L., Machlus, M., and Schramm, A.: Strontium isotopic, chemical, and sedimentological evidence for the evolution of Lake Lisan and the Dead Sea, *Geochim. Cosmochim. Acta*, 61, 3975-3992, 1997.
- 1200 Stöckli, R., Vermote, E., Saleous, N., Simmon, R., and Herring, D.: The Blue Marble Next Generation-A true color earth dataset including seasonal dynamics from MODIS, Published by the NASA Earth Observatory, 2005.
- Swierczynski, T., Brauer, A., Lauterbach, S., Martín-Puertas, C., Dulski, P., von Grafenstein, U., and Rohr, C.: A 1600 yr seasonally resolved record of decadal-scale flood variability from the Austrian Pre-Alps, *Geology*, 40, 1047-1050, 2012.

- 1205 Tamarin-Brodsky, T. and Kaspi, Y.: Enhanced poleward propagation of storms under climate change, *Nature Geoscience*, 10, 908, 2017.
- Tarolli, P., Borga, M., Morin, E., and Delrieu, G.: Analysis of flash flood regimes in the North-Western and South-Eastern Mediterranean regions, *Natural Hazards and Earth System Sciences*, 12, 1255-1265, 2012.
- 1210 Torfstein, A. and Enzel, Y.: Dead Sea Lake Level Changes and Levant Palaeoclimate, in: *Quaternary of the Levant*, edited by: Enzel, Y., and Bar-Yosef, O., Cambridge University Press, Cambridge, 115-126, 10.1017/9781316106754.013, 2017.
- 1215 Torfstein, A., Goldstein, S. L., Kagan, E. J., and Stein, M.: Integrated multi-site U–Th chronology of the last glacial Lake Lisan, *Geochim. Cosmochim. Acta*, 104, 210-231, 2013a.
- Torfstein, A., Goldstein, S. L., Stein, M., and Enzel, Y.: Impacts of abrupt climate changes in the Levant from Last Glacial Dead Sea levels, *Quaternary Science Reviews*, 69, 1-7, 2013b.
- 1220 Torfstein, A., Gavrieli, I., Katz, A., Kolodny, Y., and Stein, M.: Gypsum as a monitor of the paleo-limnological–hydrological conditions in Lake Lisan and the Dead Sea, *Geochim. Cosmochim. Acta*, 72, 2491-2509, 2008.
- Torfstein, A., Haase-Schramm, A., Waldmann, N., Kolodny, Y., and Stein, M.: U-series and oxygen isotope chronology of the mid-Pleistocene Lake Amora (Dead Sea basin), *Geochim. Cosmochim. Acta*, 73, 2603-2630, 2009.
- 1225 Torfstein, A., Goldstein, S. L., Kushnir, Y., Enzel, Y., Haug, G., and Stein, M.: Dead Sea drawdown and monsoonal impacts in the Levant during the last interglacial, *Earth Planet. Sci. Lett.*, 412, 235-244, 2015.
- 1230 Torrence, C. and Compo, G. P.: A practical guide to wavelet analysis, *Bulletin of the American Meteorological society*, 79, 61-78, 1998.
- Tsvieli, Y. and Zangvil, A.: Synoptic climatological analysis of ‘wet’ and ‘dry’ Red Sea troughs over Israel, *International journal of climatology*, 25, 1997-2015, 2005.
- 1235 Tubi, A. and Dayan, U.: Tropical Plumes over the Middle East: Climatology and synoptic conditions, *Atmospheric Research*, 145, 168-181, 2014.
- Tyrlis, E., Lelieveld, J., and Steil, B.: The summer circulation over the eastern Mediterranean and the Middle East: influence of the South Asian monsoon, *Climate Dynamics*, 40, 1103-1123, 2013.
- 1240 Vautard, R. and Ghil, M.: Singular spectrum analysis in nonlinear dynamics, with applications to paleoclimatic time series, *Physica D: Nonlinear Phenomena*, 35, 395-424, 1989.
- 1245 Waldmann, N., Neugebauer, I., Palchan, D., Hadzhiivanova, E., Taha, N., Brauer, A., and Enzel, Y.: Sedimentology of the Lacustrine Formations in the Dead Sea Basin, in: *Quaternary of the Levant: Environments, Climate Change, and Humans*, edited by: Enzel, Y., and Bar-Yosef, O., Cambridge University Press, Cambridge, 83-90, DOI: 10.1017/9781316106754.009, 2017.
- 1250 ~~Weber, N., Lazar, B., Gavrieli, I., Yechieli, Y., and Stein, M.: Gypsum Deltas at the Holocene Dead Sea linked to Grand Solar Minima, *Geophysical Research Letters*, 10.1029/2020gl091034, 2021.~~
- Welch, P. D.: The use of fast Fourier transform for the estimation of power spectra: A method based on time averaging over short, modified periodograms, *IEEE Transactions on audio and electroacoustics*, 15, 70-73, 1967.
- 1255 Witt, A., Malamud, B. D., Mangili, C., and Brauer, A.: Analysis and modelling of a 9.3 kyr palaeoflood record: correlations, clustering, and cycles, *Hydrology and Earth System Sciences*, 21, 5547-5581, 10.5194/hess-21-5547-2017, 2017.
- Yosef, Y., Aguilar, E., and Alpert, P.: Changes in extreme temperature and precipitation indices: using an innovative daily homogenized database in Israel, *International Journal of Climatology*, 39, 5022-5045, 2019.
- 1260 Zappa, G., Hoskins, B. J., and Shepherd, T. G.: The dependence of wintertime Mediterranean precipitation on the atmospheric circulation response to climate change, *Environmental Research Letters*, 10, 104012, 2015.
- 1265 Ziv, B.: A subtropical rainstorm associated with a tropical plume over Africa and the Middle-East, *Theoretical and Applied Climatology*, 69, 91-102, 2001.

Ziv, B., Saaroni, H., and Alpert, P.: The factors governing the summer regime of the eastern Mediterranean, *International Journal of Climatology*, 24, 1859-1871, 2004.

1270

Ziv, B., Dayan, U., Kushnir, Y., Roth, C., and Enzel, Y.: Regional and global atmospheric patterns governing rainfall in the southern Levant, *International Journal of Climatology*, 26, 55-73, 2006.

Zolitschka, B., Francus, P., Ojala, A. E., and Schimmelmann, A.: Varves in lake sediments—a review, *Quaternary Science Reviews*, 117, 1-41, 2015.

1275